Agricultural Water Management 320 (2025) 109873

Contents lists available at ScienceDirect

Agricultural Water Management

journal homepage: www.elsevier.com/locate/agwat

Assessing microtensiometers for monitoring stem water potential in mandarin (*Citrus reticulata* Blanco) orchard under different irrigation regimes

Girolamo Vaccaro [a], Mariachiara Fusco [a], Vincenzo Alagna [a,*], Loris Franco [b], Antonio Motisi [a], Massimo Iovino [a]

[a] Dept. of Agricultural, Food and Forest Sciences (SAAF), Univ. of Palermo, Viale delle Scienze, Bldg. 4, Palermo 90128, Italy
[b] Irritec S.p.A., Via Gambitta Conforto, Capo D'Orlando, ME 98071, Italy

ARTICLE INFO

Keywords:
Stem potential
Microtensiometer
Scholander pressure chamber
Irrigation regimes
Subsurface drip irrigation
Micro-sprinkler irrigation

ABSTRACT

Stem water potential (Ψ_{stem}) is the standard indicator of crop water status, commonly estimated using the Scholander pressure chamber (PC). However, it does not allow continuous monitoring, limiting real-time decision-making. The recently developed microtensiometer (MT) offers continuous Ψ_{stem} monitoring, overcoming the PC limitations. This study assesses the MT's reliability in monitoring Ψ_{stem} dynamics in a mandarin orchard in Sicily, Italy, under two irrigation regimes: i) a frequent irrigation regime via subsurface drip irrigation (SDI) system, employed to ensure well-watered conditions, and ii) an ordinary irrigation management typical of the area, provided by a micro-sprinkler (SPR) system. Over two seasons, Ψ_{stem} measurements obtained with the MT (Ψ_{mt}) were compared with those from the PC (Ψ_{pc}). Shading trials were also conducted to evaluate the sensor's ability to detect the plant reactions to external perturbations. A step-change in solar radiation imposed by artificial shading revealed different signal dynamics of MT sensors compared to pressure chamber Ψ_{pc} measurements, characterised by a 4-fold increase in signal time constant. This led to a consequential impact on Ψ_{stem} estimation, resulting in both a substantial time lag and attenuation, consistent with first-order sensor dynamics. Across both seasons and irrigation regimes, daily Ψ_{mt} overestimated Ψ_{stem} compared to Ψ_{pc}, along with a clear time lag coherent with the first-order response shown by the sensor-tree-complex. Under the SDI irrigation regime, Ψ_{mt} was significantly correlated with vapour pressure deficit, indicating a strong plant-atmosphere coupling under stable soil moisture conditions. Normalised cross-correlation analysis between reference evapotranspiration and Ψ_{mt} showed variable time lags, specifically in the SPR plot, subjected to alternating soil moisture conditions. These findings suggest that MTs are a promising tool for real-time monitoring of mandarin water status. However, the first-order dynamics of the sensor-tree-complex response signal preclude the use of Ψ_{mt} as a direct replacement for pressure-chamber Ψ_{stem} measurements. Consequently, suitable compensation protocols accounting for a large time constant should be developed to apply Ψ_{mt} readings to currently published crop-specific Ψ_{stem} thresholds for irrigation scheduling protocols.

1. Introduction

Efficient water management is crucial for irrigated agriculture, particularly in light of climate change and increasing water scarcity in arid and semi-arid areas (Galindo et al., 2018). The expected intensification of drought events under climate change scenarios is expected to increase crop stress due to rising thermal gradients and reduced precipitation, negatively affecting agricultural productivity (Ciais et al., 2005). For citrus crops in a Mediterranean semi-arid environment, yield success relies heavily on adequate irrigation (Rallo et al., 2017). Therefore, to optimise the productivity of citrus orchards, it is essential to manage the available water resources sustainably and, at the same time, also consider their potential cultivation under water shortage conditions.

One of the most water-efficient and precise methods of surface irrigation systems is drip irrigation, which can minimise water losses due to

* Corresponding author.
E-mail address: vincenzo.alagna01@unipa.it (V. Alagna).

https://doi.org/10.1016/j.agwat.2025.109873
Received 15 May 2025; Received in revised form 29 September 2025; Accepted 2 October 2025
Available online 8 October 2025

evaporation, surface runoff, and deep percolation (Ravikumar, 2023; Singh and Su, 2022). Unlike drip irrigation systems, subsurface drip irrigation (SDI) systems are characterised by buried emitters, effectively reducing water loss due to evaporation (Cahn and Hutmacher, 2024; Camp, 1998; Provenzano, 2007). Lamm et al. (2021) summarised recent research progress of SDI systems (from 2010 to 2020). They highlighted SDI's advantages, including high water use efficiency, uniform water application and the ability to apply water and nutrients directly and efficiently within the crop root zone compared to other systems, such as sprinkler irrigation.

Optimising water use efficiency requires selecting and designing appropriate irrigation systems and implementing management practices that supply water in volumes precisely aligned with crop water requirements. A fundamental aspect of fine-tuning irrigation scheduling is understanding the plant water status. Several studies have specifically highlighted the importance of stem water potential (Ψ_{stem}), which is widely recognised as the key indicator of a plant's water status and a valuable index for making irrigation decisions (Choné, 2001; Jones, 2004; Ortuño et al., 2006). Stem water potential assessments are typically conducted at pre-dawn or midday. In citrus trees, which exhibit low resistance to water stress, irrigation scheduling is often guided by plant water stress thresholds, with midday Ψ_{stem} values commonly ranging between −1.3 and −1.5 MPa (Ballester et al., 2011; García--Tejero et al., 2010; Gonzalez-Altozano and Castel, 1999).

Traditionally, Ψ_{stem} is estimated with the Scholander pressure chamber (Scholander et al., 1965). Although this is a reliable measurement, it is destructive, time-consuming, and does not provide real-time continuous data on the plant water status. Additionally, Levin (2019) investigated several factors affecting the pressure chamber (PC) method, including the impact of re-cutting the petiole before placing the leaf in the chamber, the period between sample excision and pressurisation, the sample equilibration duration, and the operator's influence. The operator's effect consistently outweighed the other effects, thus demonstrating that proper training of technicians is crucial for achieving reliable and accurate estimations of Ψ_{stem} by the PC technique (Ψ_{pc}).

Physiologically, certain species, such as mandarin trees, are less drought-tolerant than other crops, primarily due to their low hydraulic conductance (Romero-Trigueros et al., 2021). Water stress can lead to cavitation-induced embolism in the xylem (Hacke and Sperry, 2001; Poggi et al., 2007), reducing xylem flow and weakening the hydraulic connection between the trunks and stems. While this phenomenon is reversible, it plays a crucial role in regulating transpiration in plants under water stress (Clearwater and Goldstein, 2005). For such crops, Ψ_{pc} may be prone to inaccuracies, failing to reflect the actual water status.

The practical limitations of the PC technique impede its application for determining optimal irrigation timing and management. However, in the context of precision irrigation or plant stress diagnostics, continuous monitoring of plant water status is of utmost importance; thus, research efforts have increasingly focused on enhancing existing devices and developing new technologies for easily and accurately monitoring plant water status.

Over the years, various plant-based monitoring technologies, including sap flow probes, leaf pressure probes and psychrometers for measuring plant water potential, have been developed to enhance irrigation management.

Sap flow measurement is a widely used method for directly quantifying plant water use and transpiration by assessing water transport within the vascular system. Unlike indirect methods, which rely on environmental parameters, this technique provides accurate, plant-based physiological data, enabling precise irrigation scheduling tailored to actual plant water requirements and significantly reducing water waste (Capurro et al., 2024; Mancha et al., 2021; Venturin et al., 2020). However, sap flow methods have inherent limitations. They are primarily applicable to woody species, and their measurement accuracy can be compromised by natural temperature gradients, radial variations in sap flow, and the selection of data-processing methods, all of which introduce uncertainty (Rabbel et al., 2016). Furthermore, upscaling from individual tree measurements to whole stands requires careful sampling strategies and precise quantification of sapwood area, as variability among trees can be substantial (Lundblad et al., 2001).

The ZIM-probe method measures leaf turgor pressure using a highly sensitive pressure sensor, which is clamped to a leaf and evaluates the pressure transfer function across a patch of intact leaf tissue, showing an inverse correlation with turgor pressure (Zimmermann et al., 2008). The ZIM-probe has been recognised as a user-friendly and easily installable technique, offering significant potential for field application by growers (Fernández, 2014). However, limitations include the need for accurately species-specific calibration to interpret turgor pressure, as well as potential variability due to microclimate effects and leaf anatomical differences across different canopy positions (Bader et al., 2014; Martínez-Gimeno et al., 2017).

Recognising the importance of Ψ_{stem} as a key indicator of crop water status, various sensors have been developed to facilitate its continuous measurement. Among these, the thermocouple psychrometer emerges as an effective device for assessing Ψ_{stem} by employing psychrometric principles to determine the water potential in stem tissue through vapour pressure measurements. This sensor provides real-time data and has been proven to monitor water potential reliably (Dainese et al., 2022). However, despite its reliability, the thermocouple psychrometer has several drawbacks, including the necessity for calibration with standard solutions, a challenging installation procedure, and relatively high costs (Quick et al., 2016). The relative humidity of the air surrounding the sensing junction is crucial, as it significantly influences the temperature difference between the wet sensing junction and the dry reference junction (Rawlins, 1966). Moreover, its accuracy can decline under relative humidity nearing vapour saturation, corresponding to water potential values approaching zero (Bulut and Leong, 2008).

More recently, Pagay et al. (2014) developed the so-called micro-tensiometer (MT), a device capable of measuring water potentials of external matrices below −10 MPa, using a microelectromechanical pressure sensor. The MTs, which are inserted directly into the plant tissue, represent an innovative technology for continuous real-time monitoring of stem water potential (Ψ_{mt}). Several studies have assessed the performance of MTs under field conditions for different crops, including kiwifruit (Di Biase et al., 2025), cotton (Christenson et al., 2024), pear (Blanco and Kalcsits, 2023), nectarine (Conesa et al., 2023), and grapevines (Pagay, 2022).

Despite their successful use in other crops, the application of MTs to mandarin species remains unexplored. Citrus orchards are one of the best-adapted tree species to Mediterranean environments. Traditionally, in Sicily, mandarin orchards have been irrigated using under-canopy micro-sprinkler (SPR) irrigation systems with low-frequency scheduling. However, due to the region's semi-arid climate and frequent water scarcity, there is a growing shift toward adopting more efficient irrigation technologies, such as the SDI system, to enhance water use efficiency.

The main objective of this study was to fill the existing knowledge gap regarding the potential benefits of using MTs to monitor Ψ_{stem} of mandarin trees under Mediterranean climate conditions, within the framework of precision irrigation. For this purpose, MT performance was tested under two irrigation regimes: a frequent irrigation regime to ensure a well-watered condition maintained through an SDI system, and an ordinary irrigation management typical of the growing area, provided by a SPR system. Specific objectives also aimed at analysing (i) the accuracy of Ψ_{mt} in comparison with the established Ψ_{pc}, (ii) the MT's ability to detect plant reaction to external perturbations induced by shading trials, and (iii) the sensitivity of Ψ_{mt} values to varying climatic conditions.

2. Materials and methods

2.1. Experimental site

The experiment was conducted during the 2022 and 2023 irrigation seasons in a 30-year-old mandarin orchard (*Citrus reticulata* Blanco cv. Tardivo di Ciaculli grafted onto *Citrange* "Carrizo"), spaced 5 × 5 m and located near Palermo, Italy (38°4′53.4″ N, 13°25′8.2″ E). The climate is classified as Csa under the Köppen-Geiger system, indicating a warm temperate humid climate with hot, dry summers. The mean annual temperature reaches approximately 17 °C, while average annual rainfall amounts to 655 mm, primarily concentrated during the autumn and winter seasons.

The mandarin orchard is divided into two plots, with one representative tree selected in each plot to monitor stem water potential under different irrigation regimes. One plot has been equipped with a subsurface drip irrigation system (SDI plot) since 2018 to improve water use efficiency (Fig. 1, red polygon). To check that the tree was under well-watered conditions for the duration of the irrigation season, a 0.60 m long "Drill & Drop" probe (Sentek Pty Ltd., Stepney, Australia) was positioned 0.3 m from a single emitter and approximately 0.8 m from the tree trunk (Fig. 1). The probe measured both volumetric soil water content (SWC) and temperature from the surface to a depth of 0.60 m at 0.10 m intervals with data recorded every 20 min. The second plot (Fig. 1, green polygon) uses a traditional under-canopy micro-sprinkler irrigation system (SPR plot) commonly employed in Sicily for citrus orchards. In both plots, the soil (typic Rhodoxeralf) remained untilled, with weed control carried out mechanically during harvest or in summer.

The SDI plot features a relatively uniform soil texture that, according to the USDA (United States Department of Agriculture) classification, is classified as sandy clay loam or sandy loam, with a moderate gravel content in the top layer. The hydrological soil characteristics, for the 0–0.60 m depth profile, were determined using pressure plate extractors (Dane et al., 2002) for pressure head values of −1 m and −150 m. The average volumetric SWC at field capacity (θ_{fc}) and at wilting point (θ_{wp}) were 0.254 and 0.143 $cm^3\ cm^{-3}$, respectively, resulting in an available water fraction of 0.111 $cm^3\ cm^{-3}$. Soil organic matter was determined using the loss-on-ignition method (Bengtsson and Enell, 1986; Dean, 1974), yielding an average of 2.44 %. The SPR plot exhibited a more heterogeneous soil texture, ranging from clay to sandy clay loam (USDA). In the 0–0.60 m soil profile, the θ_{fc} and θ_{wp} were 0.317 and 0.195 $cm^3\ cm^{-3}$, respectively, resulting in an available water fraction of 0.122 $cm^3\ cm^{-3}$. The average soil organic matter content in this plot was higher than that of the SDI plot, reaching 3.38 %.

The SDI irrigation system features two drip lines per row, buried at a depth of 0.30 m and positioned approximately 1.1 m on both sides of the tree trunk. The drip lines are equipped with self-compensating drippers discharging 2.1 L h^{-1} at a pressure of 100 kPa (Multibar C model, Irritec®) spaced 0.5 m apart. The SPR irrigation system is characterised by two micro-sprinklers per tree, delivering a flow rate of 200 L h^{-1} at a pressure of 150 kPa, wetting an area almost corresponding to the projection of the mandarin tree canopy.

The SDI plot was managed with a high-frequency irrigation regime aimed at preventing crop water stress. At this aim, the SWC along the root zone was monitored with the Drill & Drop sensor, ensuring that the values remained consistently close to θ_{fc}. In contrast, the SPR plot was managed by the farmer following a nearly uniform, lower-frequency irrigation schedule. Irrigation events typically occurred according to a biweekly plan, unless there were no rainfall events, and water application volumes were determined by his practical experience.

2.2. Climate and micrometeorological data

Air temperature, *T* (°C), relative humidity, *RH* (%), thus vapour pressure deficit, VPD (kPa), precipitation, *P* (mm), solar radiation, *SR*

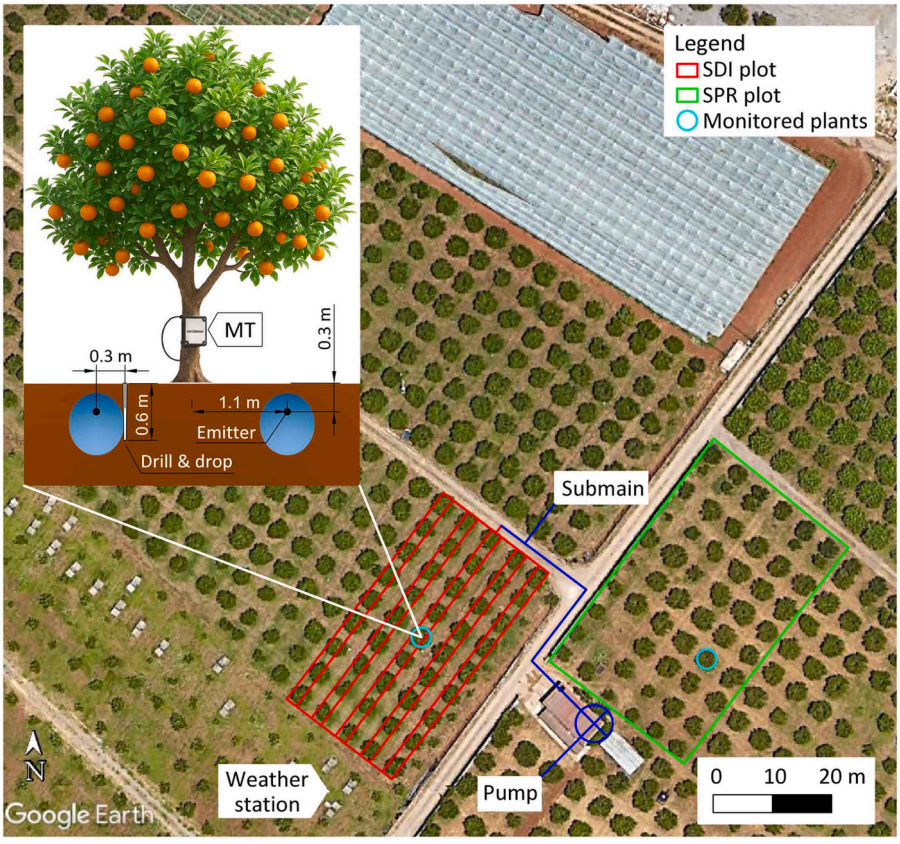

Fig. 1. Experimental layout of the SDI and SPR plots. For the SDI plot, the positions of the emitters and the soil water content probe are also displayed.

(MJ m^{-2} h^{-1}), wind speed, u (m s^{-1}) were recorded, with a time-step of 30 min, by a WatchDog 2000 series weather station (Spectrum Technologies, Inc., Aurora, IL, USA) installed inside the field (Fig. 1). The hourly average values of meteorological variables were used to estimate the hourly grass reference evapotranspiration, ETo (mm h^{-1}), using the FAO-56 Penman-Monteith equation (Allen et al., 1998).

2.3. Stem water potential estimations

Continuous monitoring of stem water potential (Ψ_{mt}) was conducted using four commercial microtensiometers (FloraPulse, Davis, CA, USA), with two sensors installed in the trunk of a representative tree in each plot. These microtensiometers (MT) were connected to the FloraPulse data logger, which automatically records Ψ_{mt} every 20 min and uploads the data to the FloraPulse cloud. Sensor calibration is not required before field installation, as each MT is individually factory-calibrated (https://www.florapulse.com/resources). The MT installation, following the manufacturer's recommendation, involved several key steps to ensure precise attachment and optimal functioning. The tree trunk phloem tissue was exposed by carefully removing the bark from a selected flat section. A stainless-steel sleeve was inserted into the trunk with a hammer to position it securely. A drill was used to penetrate the sleeve and drill into the xylem tissue, removing the tissue within. This cavity was filled with a kaolin-based mating compound to create a stable interface between the sensor and the tree's xylem. The hydrated MT was then placed into the compound. To seal the installation, a stainless-steel cap was added to close the sleeve, and the sleeve's exterior was covered with silicone to ensure an airtight and waterproof seal. Finally, thermal insulation was applied by wrapping the sensor to minimise external temperature fluctuations. The sensors equilibrated with the mandarin trunk through the mating compound within two days of installation. The collected data were then aggregated at an hourly scale, and the average values recorded from the two MT were used for analysis.

Estimation of stem water potential by Scholander pressure chamber (Ψ_{pc}) was conducted on the same mandarin trees monitored with MT, following the protocols suggested by Turner (1988). During the two irrigation seasons, Ψ_{pc} were carried out throughout the day on two healthy stems, each wrapped in an aluminium foil approximately one hour before the test, and the average value was considered. Specifically, Ψ_{pc} tests were scheduled considering the farmer's irrigation management carried out in the SPR plot, aiming to capture potential water stress three days before irrigation and to assess plant water status recovery the following day. This low-frequency irrigation management was expected to induce marked fluctuations in soil moisture and, consequently, in tree water status. In the SDI plot, Ψ_{pc} tests were performed simultaneously with those in the SPR plot, regardless of whether they occurred before or after irrigation application, since this irrigation regime involved more frequent water application. At each measurement day, Ψ_{pc} tests were performed every three hours, from 6:00 am to 06:00 pm, in the 2022 irrigation season, and every two hours, from 6:00 am to 8:00 pm, in the 2023 irrigation season.

To evaluate the short-term responsiveness of Ψ_{mt} to external perturbations, two shading experiments were conducted at the peak and end of summer to assess the sensor behaviour under different *SR* conditions. An 80 % black shading net was applied from noon on 3 August 2023 until the same time the following day. During the shading trial, Ψ_{pc} measurements were also performed at two-hour intervals from dawn to dusk. The same trial was replicated on 21–22 September.

2.4. Statistical analyses

Correlation analysis was performed using data collected simultaneously from MTs and the PC over the two experimental years to validate Ψ_{mt} against Ψ_{pc} for both irrigation regimes.

Scatter group analysis was performed to assess the correlation between Ψ_{mt} and VPD across different phases of tree diurnal water dynamics, and 90 % confidence ellipses were determined for each group for the two monitored mandarin trees under different irrigation regimes.

Time-lagged normalised cross-correlation was performed in MATLAB programming software (v.9.14.0, R2023a, The MathWorks, Inc., Natick, MA, USA) using 1-minute interpolated continuous data between ETo and Ψ_{mt}. Normalised cross-correlation assesses the correlations between two temporally shifted time series datasets (Chatfield and Xing, 2019), repeatedly computing the Pearson Product Moment Correlation (cross-correlation) Coefficient (XCC) after each shift. In this study, the resulting 'offset' values, each representing a 1-minute interval, are identified at the highest absolute normalised XCC within the series and indicate the time shift between the two specific time series. The time shift and XCC were computed on a daily basis across both seasons for the SDI and SPR irrigation regimes.

3. Results

3.1. Climate conditions, irrigation amounts, and soil water content dynamics

Maximum vapour pressure deficit (VPD_{max}), daily crop reference evapotranspiration (ETo), daily maximum air temperature (T_{max}), precipitation (P) and irrigation amounts (I) delivered in the SDI and SPR plots for the two monitored irrigation seasons (2022–2023) are shown in Fig. 2. The study period was characterised by consistently high temperatures, with T_{max} values regularly exceed 30 °C in both seasons. Extreme T_{max} peaks reached 44.2 °C in August 2022 and 45.4 °C in July 2023. However, in 2022, the variability of T_{max} increased markedly toward the end of the season, whereas in 2023, greater T_{max} variability was observed primarily during the early part of the season.

Daily ETo values were generally greater than 5.4 mm d^{-1} until early August, after which they gradually declined. Late-season peaks reached 6.0 mm d^{-1} on 17 September 2022 and 7.4 mm d^{-1} on 22 September 2023, both associated with concurrent high temperatures, low *RH*, and increased wind speed (u data not shown). For the observation periods, total ETo was 340.38 and 367.87 mm in 2022 and 2023, respectively.

VPD_{max} exhibited pronounced diurnal fluctuations in both seasons. Notably, the 2023 season experienced a higher frequency of days in July with VPD_{max} values exceeding 4 kPa and peaking up to 9 kPa, indicating a stronger atmospheric water demand compared to 2022, which showed a single extreme event on 18 August. Extreme VPD events likely intensified crop transpiration rates, thereby exposing plants to water stress conditions, particularly in the presence of limited soil moisture availability.

Rainfall during the monitoring periods consisted of three events in 2022 (15.2 mm on 12 August, 2.8 mm on 24 August, and 4.4 mm on 21 September) and two in 2023 (2.8 mm on 4 August and 8.4 mm on 6 September).

Fig. 2**b** and **d** illustrate the SPR irrigation events (blue bars) during the Ψ_{mt} monitoring period. Across the full irrigation season (June -October), the farmer applied nine irrigation events in both 2022 and 2023, corresponding to total irrigation volumes of 296.43 mm and 351.66 mm, respectively. In contrast, 59 and 54 irrigation applications were employed in the SDI plot, delivering seasonal irrigation volumes of 323.21 mm and 292.94 mm, in 2022 and 2023, respectively.

Soil water content dynamics for the SDI plot are shown in Fig. 3**a** and **b** for the 2022 and 2023 seasons, respectively. Across the 0–0.60 m soil profile, SWC values ranged from 0.160 to 0.376 cm^3 cm^{-3}. As shown, the frequent irrigation management adopted in this plot successfully maintained well-watered conditions, with average SWC consistently close to the red horizontal line representing the θ_{fc} threshold. It is noteworthy that the SWC values marked by the black arrows in Figs. 3**a** and 3**b** exhibited no appreciable variation in response to the VPD peaks recorded on 18 August 2022 (Fig. 2**a**) and 24–25 July 2023 (Fig. 2**c**), respectively. In Fig. 3**a**, the blue arrow indicates an increase in SWC resulting from a small irrigation event applied by the farmer using the

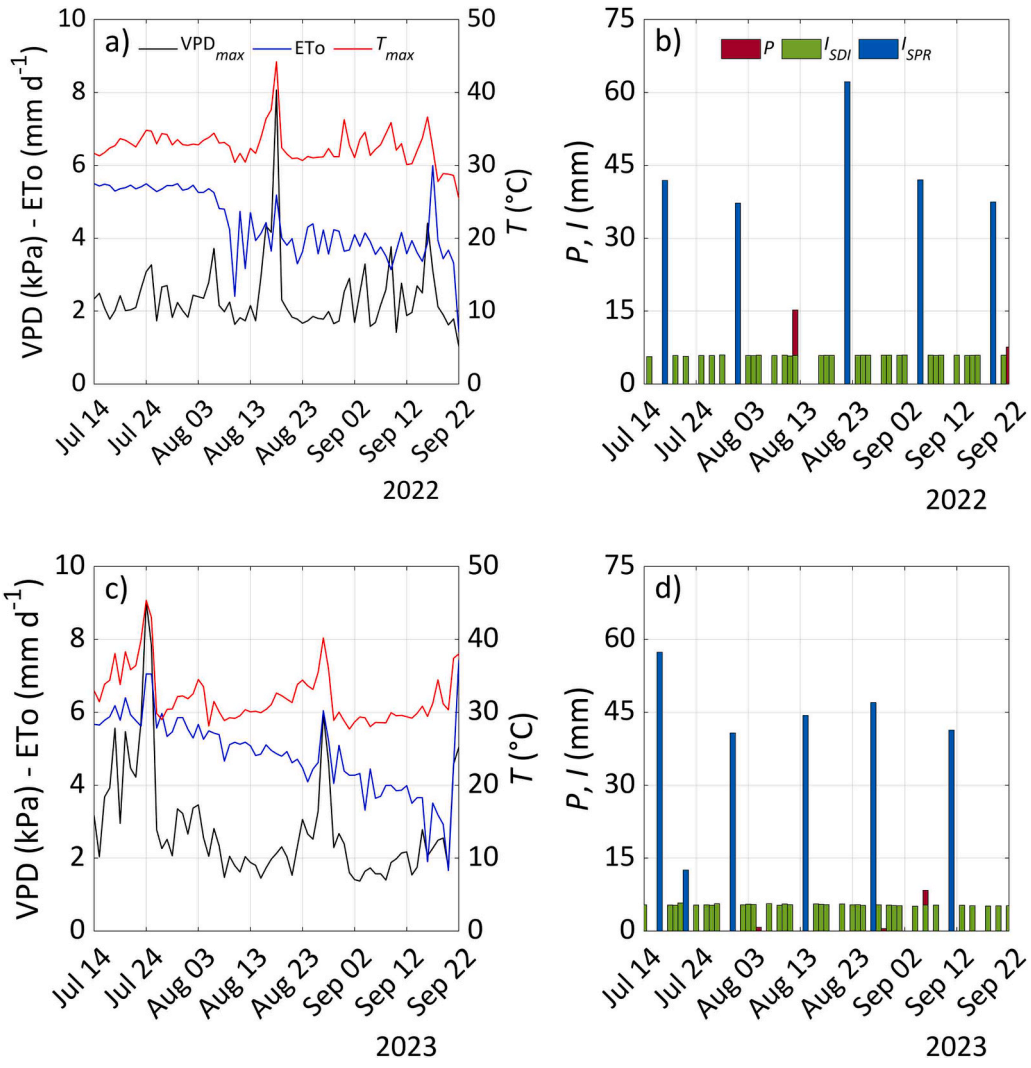

Fig. 2. Time evolution of maximum vapour pressure deficit (VPD_{max}), daily reference evapotranspiration (ETo) and maximum daily temperature (T_{max}) during **a**) the 2022 and **c**) the 2023 irrigation seasons. Precipitation (P) and irrigation amount (I) under the SDI (I_{SDI}) and SPR (I_{SPR}) irrigation regimes for **b**) the 2022 and **d**) the 2023 irrigation seasons.

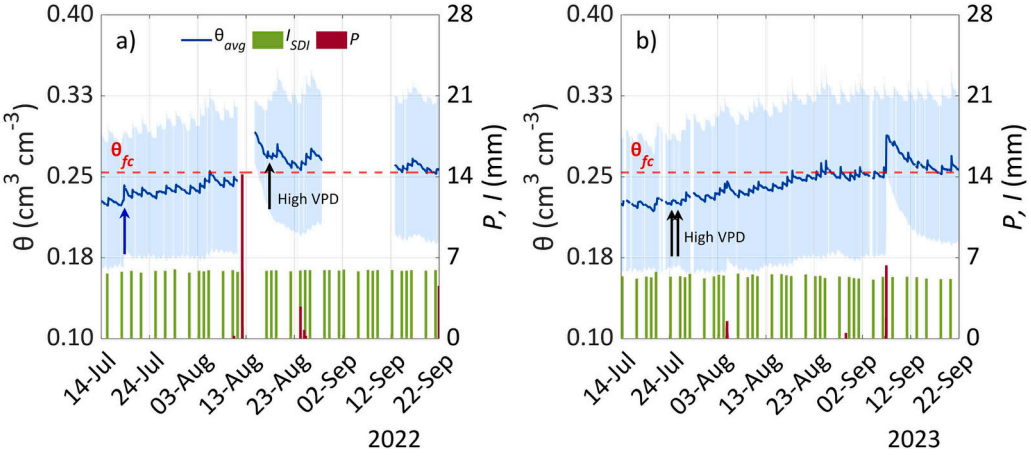

Fig. 3. Daily dynamics of the average soil water content (θ_{avg}) and its standard deviation (blue shaded area) along the 0–0.6 m soil profile within the SDI plot during **a**) the 2022 and **b**) the 2023 irrigation seasons. Irrigation events (I_{SDI}) and precipitation (P) are also shown. The red dashed horizontal line indicates the soil water content at field capacity (θ_{fc}). The blue arrow indicates a supplementary irrigation event applied by the farmer.

existing micro-sprinkler system, aimed at moistening the soil surface to facilitate mechanical weed control.

3.2. Stem water potential monitored with microtensiometer

Temporal patterns of Ψ_{mt} under frequent irrigation (via SDI) and ordinary irrigation (via SPR) regimes during the 2022 and 2023 growing seasons are shown in Fig. 4. Continuous MT monitoring revealed the difference in Ψ_{mt} dynamics between the two regimes, evident both on an hourly basis and on longer time intervals (i.e., on a day-to-day time scale). Specifically, diurnal changes in Ψ_{mt} showed the expected hourly pattern, with minimum values occurring during midday hours, corresponding to the increase in air temperature, *SR* and VPD from dawn to midday, followed by a gradual rebound of Ψ_{mt} in the afternoon and nighttime. Dependence of Ψ_{mt} on ETo, VPD and *SR* was particularly evident during the heat-wave events that occurred in both seasons. During such events, with air temperature, VPD and ETo values as high as 45°C, 8–9 kPa and 9 mm day^{-1}, respectively (Fig. 2), the lowest Ψ_{mt} values were observed (Fig. 4) for both irrigation regimes.

In the SDI plot, day-to-day changes of the Ψ_{mt} remained relatively stable compared to those recorded in the mandarin tree under the SPR regime, reflecting the stabilising effect of the high-frequency irrigation schedule, which maintained a consistent SWC across the seasons (Fig. 3). As reported in Table 1, lower coefficients of variation (*CV*) were observed in pre-dawn (Ψ_{pd}) and midday (Ψ_{md}) Ψ_{mt} compared to the SPR plot. However, Ψ_{pd} values, despite non-limiting soil water conditions, can be influenced by environmental factors. For instance, on 25 July 2023, during the heat-wave event, a high-VPD occurred (Fig. 2**c**), and the mandarin tree exhibited more negative Ψ_{pd} values (Fig. 4**b**, black arrows) compared to the preceding day, indicating an incomplete overnight recovery from atmospheric stress. The most substantial recovery occurred within the first 24 h, with increases of 40.68 % from the Ψ_{pd} value recorded during the peak stress. Full recovery to pre-event levels was achieved four days later. On the same date, Ψ_{md} reached its most negative value, equal to −2.05 MPa (Fig. 4**b**, black arrows), indicating that Ψ_{md} is also highly responsive to environmental drivers. The atypical increase in Ψ_{mt} recorded between in early 2022 season (Fig. 4**a**, blue arrow), which can be ascribed to the small irrigation event previously described, highlighs the MT sensitivity to short-term changes in plant water status.

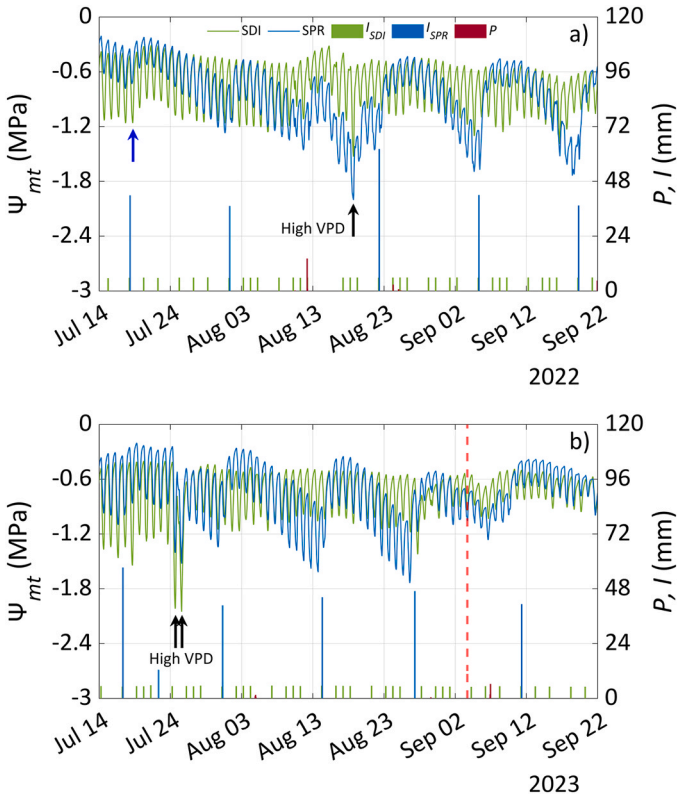

Fig. 4. Time series of Ψ_{mt} for **a**) the 2022 and **b**) the 2023 growing seasons, under both SDI and SPR irrigation regimes. Precipitation (*P*) and the corresponding irrigation events (*I*) of the SDI (I_{SDI}) and SPR (I_{SPR}) irrigation regimes are also shown. The blue arrow indicates a supplementary irrigation event applied by the farmer.

Due to the low-frequency irrigation scheduling, the day-to-day changes of hourly Ψ_{mt} values in the SPR plot were more pronounced. Indeed, *CV* values (Table 1) of Ψ_{pd} and Ψ_{md} were higher compared to the SDI plot, especially in the 2022 season. Notably, in the SPR plot, a major pruning carried out on September 3rd, 2023 (indicated by the dashed red line in Fig. 4**b**), reduced the crop transpiration (Ye et al., 2021), dampening plant water potential fluctuations.

Regarding the Ψ_{pd}, the most negative values are usually recorded on the day of the water application, as the farmer generally begins irrigating after pre-dawn. Following each irrigation event, the tree exhibited a progressive recovery of its stem water potential over the subsequent days followed by a almost linear decrease. The observed linear decline in Ψ_{mt} following the progressive soil drying, along with the onset of crop water stress, is consistent with the near-anisohydric behaviour attributed to mandarins. Unlike other citrus species, mandarins tend to lower their water potential in response to decreasing soil moisture availability within the irrigation cycle (Romero-Trigueros et al., 2021). The extent and rate of this recovery depended primarily on the initial Ψ_{pd} values before the irrigation event, which can also be influenced by external factors such as VPD. Table 2 shows all pre-irrigation Ψ_{pd} values for SPR plot, together with the corresponding daily percentage recovery relative to the pre-irrigation condition. In all water applications, Ψ_{pd} showed a marked recovery on the first day after the irrigation event, followed by a reduced rate of recovery over the subsequent days. In the most stressed periods, maximum recovery increases up to 40 % of the initial value (Table 2, bold values) with the highest recovery rate after one day (43.1 %) when the most negative initial Ψ_{pd} values (e.g., −1.32 MPa) occurred. Additionally, the effect of irrigation ends within the first 24–48 h, after which the recovery tends to stabilise or decline. Notably, the sharp decrease of −166.94 % is attributable to the VPD peak event that occurred in 2023 (Fig. 2**c**), which likely counteracted the benefits of irrigation. Following this extreme event, Ψ_{pd} did not return to its pre-event level until the subsequent water application (Fig. 4**b**), suggesting a plant's hydraulic dysfunction. The most negative Ψ_{pd} (-1.31 MPa) and Ψ_{md} (-2.00 MPa) values (Fig. 4**a**, black arrow) recorded in the SPR plot were again attributed to the high VPD and ETo levels observed during a heat-wave event, in this case registered on 18 August 2022 (Fig. 2**a**), when the farmer withheld irrigation due to a preceding rainfall event.

3.3. Microtensiometer vs pressure chamber

An example of the daily patterns of stem water potential estimated using the pressure chamber (Ψ_{pc}) and the microtensiometer (Ψ_{mt}) along with vapour pressure deficit (VPD), over two days of the 2023 season for both irrigation regimes is illustrated in Fig. 5. The data refer to Ψ_{pc} tests conducted three days before (Fig. 5**c**) and one day after (Fig. 5**d**) the irrigation event in the SPR plot; the simultaneous tests performed in the frequently irrigated SDI plot are representative of post-irrigation (Fig. 5**a**) and pre-irrigation (Fig. 5**b**). Both MT and PC methods effectively distinguished the impacts of the two different irrigation regimes on tree water status, showing significant differences in stem water potential under similar VPD conditions. In general, Ψ_{mt} values were consistently less negative than Ψ_{pc} values, with the differences between the two methods being greater in the afternoon and more pronounced before irrigation (Fig. 5**b** and **c** for SDI and SPR irrigation regimes, respectively).

Table 1
Summary statistics of stem water potential at predawn, Ψ_{pd} (MPa), and midday, Ψ_{md} (MPa), for SDI and SPR systems across both 2022 and 2023 irrigation seasons.

Statistics	2022				2023			
	SDI		SPR		SDI		SPR	
	Ψ_{pd}	Ψ_{md}	Ψ_{pd}	Ψ_{md}	Ψ_{pd}	Ψ_{md}	Ψ_{pd}	Ψ_{md}
Min	−0.71	−1.53	−1.31	−2.00	−0.87	−2.05	−0.98	−1.74
Max	−0.31	−0.71	−0.21	−0.52	−0.40	−0.69	−0.20	−0.68
Mean	−0.48	−1.08	−0.61	−1.06	−0.53	−1.07	−0.52	−1.05
δ	0.09	0.14	0.26	0.36	0.08	0.23	0.19	0.27
CV (%)	18.22	13.00	41.81	33.50	15.88	21.65	36.73	25.61

Table 2
Daily percentage recovery of predawn stem water potential, $\%\Delta\Psi_{pd}$ (t), relative to the Ψ_{pd} pre-irrigation condition for both irrigation seasons in the SPR plot.

Year	Date	Ψ_{pd} pre-irrig. (MPa)	$\%\Delta\Psi_{pd}$ (t)						
			$t=1$	$t=2$	$t=3$	$t=4$	$t=5$	$t=6$	$t=7$
2022	18 Jul	−0.35	24.54	10.90	−2.14	−6.79	−10.36	−7.94	−12.46
	1 Aug	−0.74	**28.42**	8.50	−1.17	−4.80	−7.84	−12.29	−7.01
	22 Aug	−0.98	**35.00**	12.11	5.71	2.08	−0.68	−2.81	−4.38
	5 Sep	−1.24	**43.11**	15.49	4.37	−2.54	0.71	−0.23	−5.31
	19 Sep	−1.32	**43.72**	11.91	5.26	4.23	2.37	−0.32	−1.27
2023	17 Jul	−0.34	26.84	13.64	−7.44	−5.10	−9.39	6.52	2.83
	22 Jul	−0.28	8.01	3.48	−166.94	82.81	−7.63	7.50	−3.14
	31 Jul	−0.62	43.23	14.82	−1.54	−2.17	−12.59	−7.66	−7.90
	14 Aug	−0.90	**40.75**	16.95	3.36	−1.53	−6.90	−5.46	−8.83
	27 Aug	−0.73	**18.59**	9.59	2.37	−4.35	−6.52	−15.68	−0.15
	11 Sep	−0.41	4.31	−0.33	−1.90	−5.88	−9.88	−0.64	−5.93

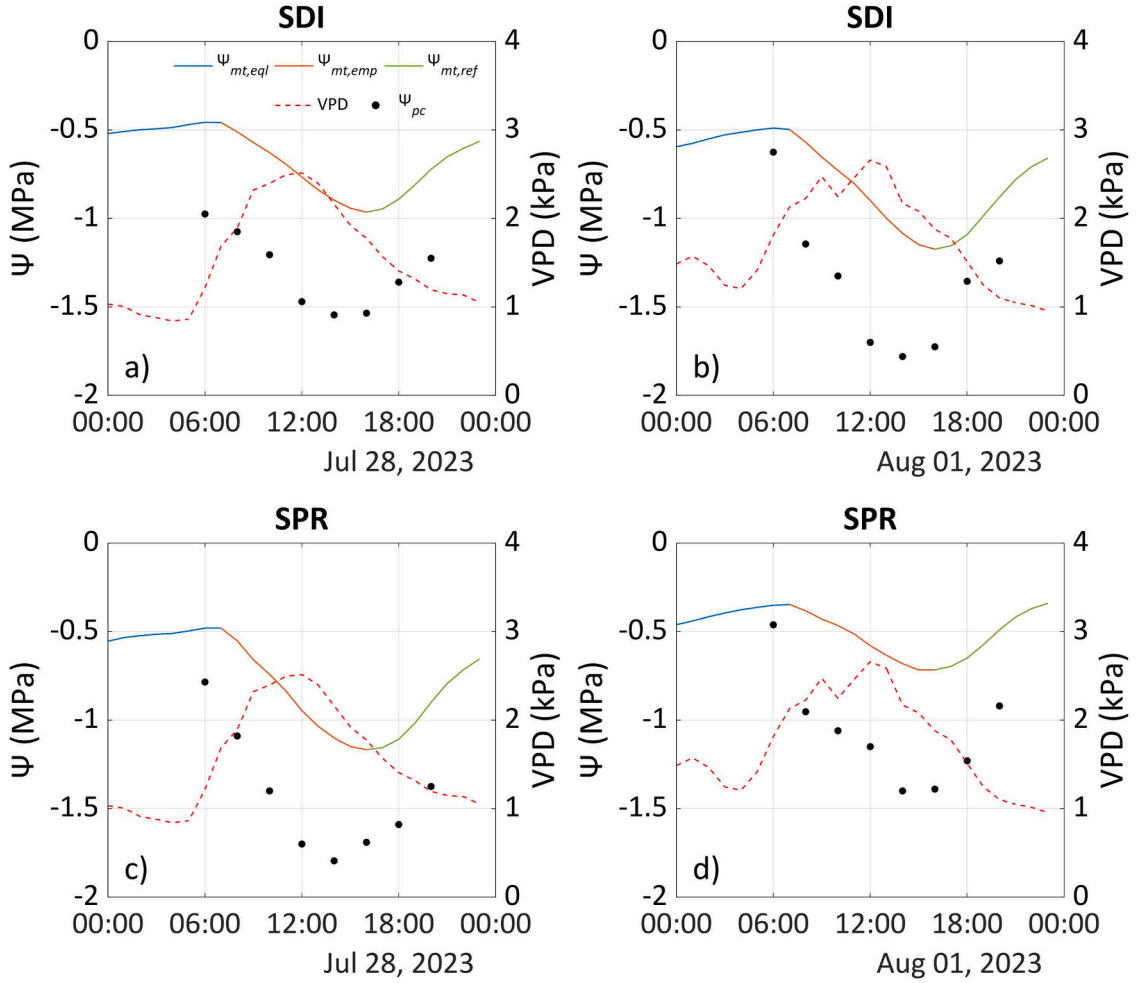

Fig. 5. Daily dynamics of Ψ_{pc} and Ψ_{mt} at the equilibrium ($\Psi_{mt,eql}$), emptying ($\Psi_{mt,emp}$) and refilling ($\Psi_{mt,ref}$) phases under SDI and SPR irrigation regimes. Vapour pressure deficit (VPD) data are also plotted.

For both irrigation regimes, the most negative values of the Ψ_{pc} were usually recorded at 14:00. Conversely, the minimum value of the Ψ_{mt} generally occurred approximately two hours later, emphasising a certain time lag between the two methods. Additionally, the higher VPD were recorded at midday on both sampling days, further indicating a time lag of two and four hours between the atmospheric water demand and Ψ_{pc} and Ψ_{mt}, respectively.

Daily pattern of Ψ_{mt} provides to identify the well-known three distinct time slots of plant water dynamics (Fig. 5): (i) the equilibrium phase (00:00–07:00, blue line), (ii) the emptying phase (08:00–16:00, orange line), and (iii) the refilling phase (17:00–23:00, green line). These time slots and/or phases were used to assess the scatter group analysis between Ψ_{mt} and VPD, which is discussed in the next Section.

Fig. 6 illustrates the two shading experiments conducted under similar conditions of solar radiation (*SR*) to assess the ability of Ψ_{mt} and Ψ_{pc} to evaluate the plant reaction to covering and uncovering with a black shade net. The MTs responded readily to the shading experiment, especially during the peak of summer (Fig. 6**a** and **b**), in contrast to the attenuated response observed at the end of summer (Fig. 6**c** and **d**). This dynamic was evident from the change in the slope of the Ψ_{mt} vs time relationship, which decreased after covering and increased after uncovering. The application of the shade net resulted in consistently less negative Ψ_{mt} values during the covered intervals, as a consequence of the physiological response to reduced transpiration demand due to decreased incident *SR*. Upon removal of the shade, Ψ_{mt} immediately declined, as a consequence of an increase in transpiration rate and a swift shift in plant water status, suggesting a prompt responsiveness of the MT to the microclimate change. Similar trends were observed for Ψ_{pc} in both shading experiments. Compared to Ψ_{mt}, Ψ_{pc} remained responsive to changes in microclimatic conditions even in late summer. It is worth noting that, following the disturbance events, Ψ_{pc} values remained consistently more negative than Ψ_{mt}. This divergence is related to the dynamics of both Ψ_{mt} and Ψ_{pc} at the time of disturbance: at the moment of covering, Ψ_{stem} was in the decreasing stage within the diurnal cycle and shading halted the decreasing trend of Ψ_{stem}. This effect was observed using both techniques (MT or PC), but with a different dynamic. The Ψ_{pc} stabilised almost immediately, while the Ψ_{mt} displayed a more gradual response, slowing down but continuing to decrease for up to four hours before stabilising (Figs. 6**a** and 6**c**). Interestingly, these contrasting dynamics were evident not only during the transition from full sunlight to shade but also upon shade to full sunlight. Ψ_{pc} decreased almost immediately after exposure to sunlight (Fig. 6**b** and **d**), reaching a minimum within two hours; in contrast, Ψ_{mt} showed a slower response, reaching the minimum 4–5 h later.

To further characterise the dynamic response of the sensor-tree complex, an approximate estimation of the time constant (τ), defined as the time required to reach 63 % of the change following a disturbance in a first-order system (Nobel, 2009; Phillips et al., 2004), was calculated for both Ψ_{mt} and Ψ_{pc}. The calculation was limited to the uncovering phase of the experiment performed at the peak of summer (3–4 August session, Fig. 6**b**), when the dynamics of the changes were sufficiently large. For Ψ_{pc}, 63 % of the change occurred 29 and 32 min after disturbance (sunlight exposure), respectively, in SDI and SPR; in contrast, Ψ_{mt} reached 63 % of the total change after 122 and 125 min

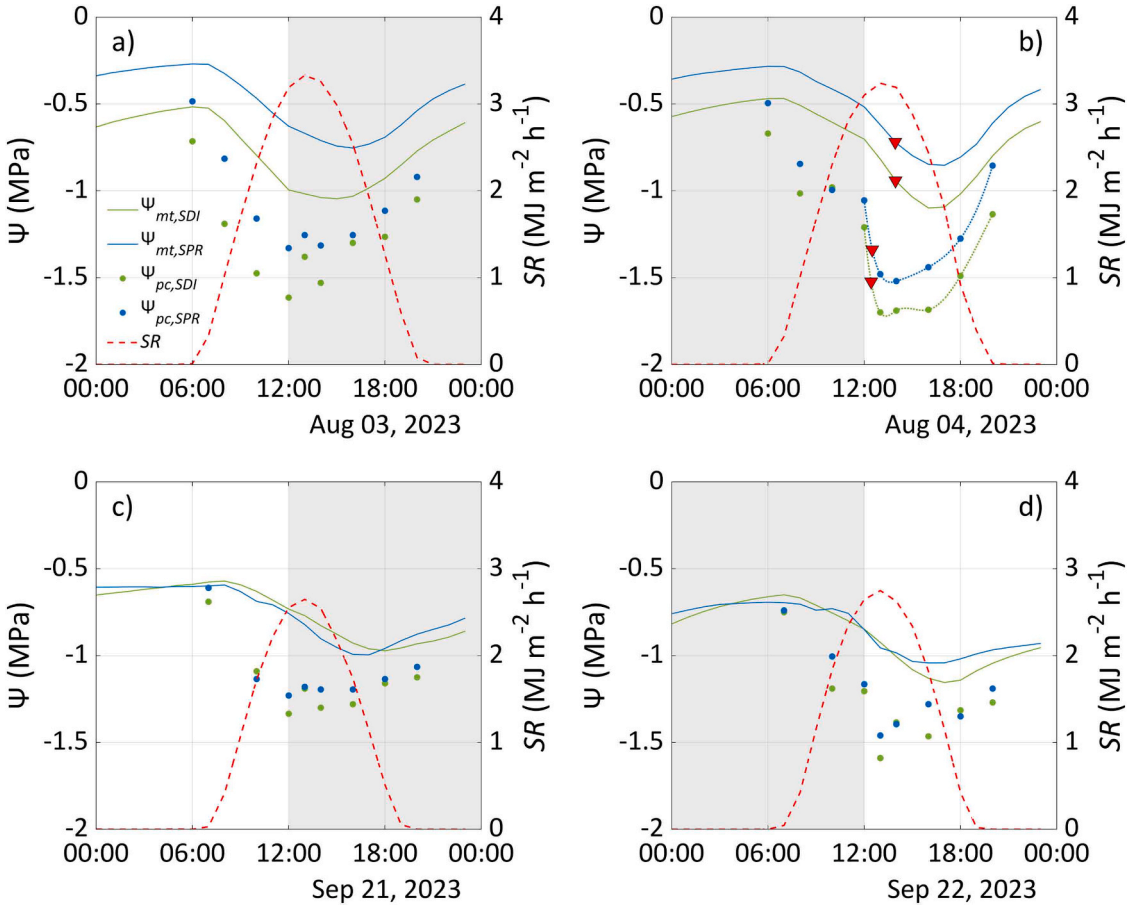

Fig. 6. Daily evolution of Ψ_{mt} and Ψ_{pc} under the SDI ($\Psi_{mt,SDI}$ and $\Psi_{pc,SDI}$, respectively) and the SPR ($\Psi_{mt,SPR}$ and $\Psi_{pc,SPR}$, respectively) irrigation regimes, along with solar radiation (*SR*) levels during the shading tests. The grey areas correspond to the trees' shading period. For both irrigation regimes, red triangles represent the Ψ_{stem} values of both PC and MT methods at their respective time constants (τ), defined as the time following a disturbance when 63 % of the total change has been recorded.

(Fig. 6**b**, filled triangles).

Linear regression analysis was performed between Ψ_{mt} and Ψ_{pc} for the SDI and SPR irrigation regimes, pooling the data collected in the two irrigation seasons. The relationship between Ψ_{mt} and Ψ_{pc} exhibited similar slopes and coefficient of determination, with R^2 of 0.62 ($p < 0.0001$) in the SDI plot (Fig. 7**a**) and R^2 of 0.63. ($p < 0.0001$) in the SPR plot (Fig. 7**b**), showing a significant relationship between the Ψ_{stem} estimated by the two methods. However, the relationship between Ψ_{mt} and Ψ_{pc} deviated from the identity line, especially for the SDI plot, with more negative values for Ψ_{pc} compared to Ψ_{mt} (Fig. 7**a**).

3.4. Correlation between Ψ_{mt} and vapour pressure deficit

Fig. 8 shows the relationship between Ψ_{mt} and VPD under SDI and SPR irrigation regimes using scatter plots of hourly data collected in both years during the monitoring period. The scatterplots generally align with the expected negative relationship between Ψ_{mt} and VPD. However, the two irrigation regimes exhibited different levels of dispersion, with the frequently irrigated SDI (Fig. 8**a** and **c**) showing lower variability than the ordinary irrigated SPR plot (Fig. 8**b** and **d**). In the SDI plot, where SWC remained consistently stable over time (Fig. 3**a** and **b**), Ψ_{mt} showed a strong sensitivity to VPD. This relationship was particularly evident in the 2022 season, in which VPD variability was comparatively lower ($R^2 = 0.57$, $p < 0.0001$; Fig. 8**a**). Conversely, in the SPR irrigation regime, Ψ_{mt} displayed weaker correlations with VPD, indicating a stronger influence of SWC on Ψ_{mt} dynamics.

Further analysis of the scatterplots shows that, even at the same VPD level, Ψ_{mt} values vary depending on the time of day. Specifically, higher water potential values were recorded in the early morning, while the lowest values were observed during midday and early afternoon. To capture these diurnal dynamics, data were divided into the three distinct time slots mentioned before. For each time slot, a 90 % confidence ellipse was calculated to better visualise the distribution of data. These phases reflect the tree's water dynamics throughout the day: an equilibrium phase in which stem and soil water potentials are balanced under minimal transpiration (Yang et al., 2013; Zhang et al., 2023); an emptying phase in which increasing VPD drives water loss from plant reserves; and a refilling phase in which decreasing VPD allows plants to replenish water stores (Phillips et al., 2004; Vogel et al., 2017).

The analysis showed significant variation between the time slots and the irrigation regimes across both seasons. In the SDI irrigation regime and for both seasons (Fig. 8**a** and **c**), Ψ_{mt} vs VPD values recorded in the equilibrium phase exhibit a small size of the ellipse, especially in the 2023 irrigation season (Fig. 8**c**), indicating more concentrated data around the mean (-0.54 MPa for the 2022 season and −0.58 MPa for the 2023 season). For the emptying phase, the ellipse is larger than in the equilibrium phase, suggesting greater variability in the data. For the refilling phase, a more elongated ellipse is shown, indicating a stronger correlation between Ψ_{mt} and VPD ($R^2 = 0.70$ for both irrigation seasons). In the SPR irrigation regime and for both seasons (Fig. 8**b** and **d**), the sizes of the ellipses of the three distinct time slots are larger than in the SDI plot, suggesting less predictability in the data, with a weaker correlation between Ψ_{mt} and VPD, due to circular shapes of the ellipses, especially in the 2022 irrigation season (Fig. 8**b**). Moreover, the data are more diffusely and irregularly distributed, reflecting greater variability within the group.

3.5. Sensitivity of Ψ_{mt} to reference evapotranspiration

Time-lagged normalised cross-correlation analysis was used to examine the interpolated 1-minute time series (Phillips et al., 1997, 2004) datasets of ETo and Ψ_{mt} for SDI and SPR irrigation regimes across the 2022 and 2023 growing seasons. Fig. 9 illustrates the highest values of normalised cross-correlation coefficient (XCC, Fig. 9**a** and **b**), and the daily values of the time shifts (Fig. 9**c** and **d**) for both seasons. Additionally, the maximum water pressure deficit (VPD_{max}) values exceeding 6 kPa (black dashed lines), the precipitation (red dashed lines), and, only for the SPR plot, the irrigation events (blue dashed lines) are also dipsyed (Fig. 9**c** and **d**).

For both seasons, the highest XCC values declined over time in both irrigation regimes, with fluctuations on days of high VPD_{max} or rainfall. In the SPR plot, XCC also responded to farmer-applied irrigation events, and on these days, time shifts varied markedly.

To characterise the dynamic response of the sensor-tree complex over a longer period than the two-day shading trials, daily values of Ψ_{mt} time constant (Fig. 10) were estimated from the inversion of the relation between τ and the phase delay (φ), calculated from the normalised cross-correlation analysis performed against ETo, for the response of a first-order system to a sinusoidal input with angular frequency ω, according to the following equation:

$$\tau = \frac{-\tan(\varphi)}{\omega} \quad (1)$$

with ω equal to $2\pi f$ and f representing the frequency of the 24-hour diel cycle, with the simplifying assumption that ETo follows a sinusoidal pattern (Monteith and Unsworth, 2008). The analysis was limited to cloudless days of the 2022 season (Fig. 9**c**). Data are shown for a period covering and extending over a full cycle of SPR irrigations (Fig. 10).

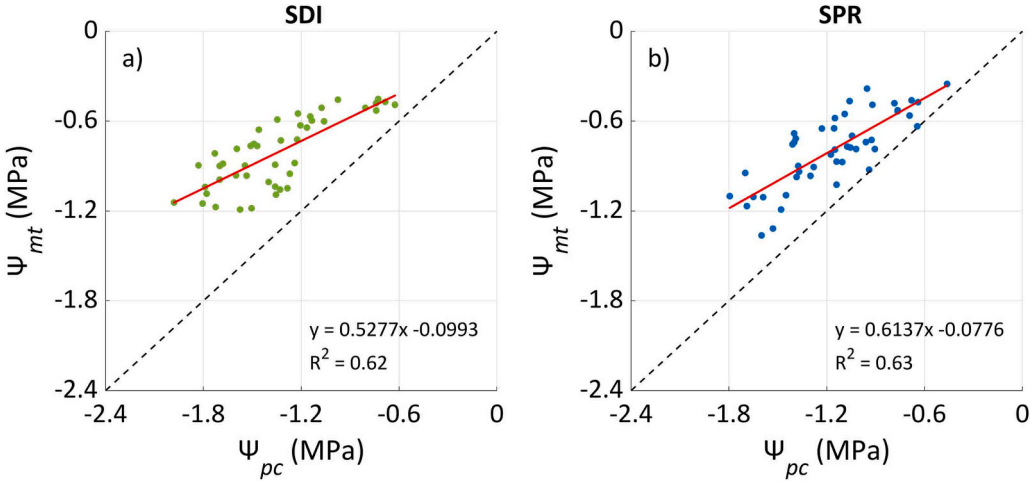

Fig. 7. Linear relationship between stem water potential estimated with the microtensiometers, Ψ_{mt}, and the pressure chamber, Ψ_{pc}, under the **a**) SDI and **b**) SPR irrigation regimes.

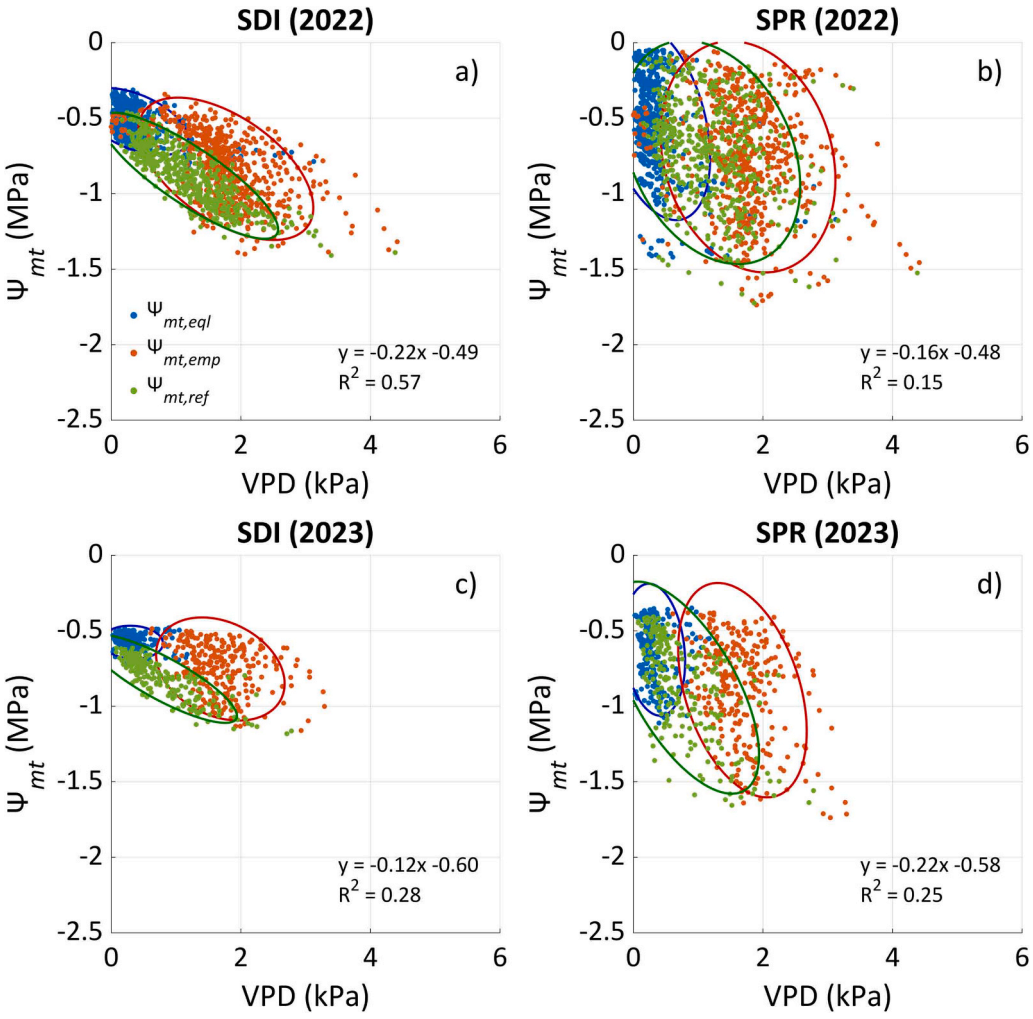

Fig. 8. Scatter group plot between Ψ_{mt} and VPD in the three distinct dynamic hydraulic phases of the tree (00:00–07:00 equilibrium, $\Psi_{mt,eql}$, 08:00–16:00 emptying, $\Psi_{mt,emp}$, and 17:00–23:00 refilling, $\Psi_{mt,ref}$) for the 2022 and 2023 irrigation seasons under (**a**, **c**) the SDI and (**b**, **d**) the SPR irrigation regimes. The ellipse function draws a 90 % confidence level for each phase group.

Over the observation period, Ψ_{mt} time constant showed a different dynamic between SDI and SPR irrigation regimes. In SDI, τ resulted fairly stable, with minor fluctuations during the observation period, whereas in SPR, daily τ changes exhibited a distinctive pattern within the irrigation cycle, decreasing progressively in the days following irrigation, then increasing sharply after the subsequent irrigation event (Fig. 10).

4. Discussion

Although this study was not specifically designed to assess water use efficiency, the differing irrigation frequencies and volumes applied generated distinct soil moisture dynamics, providing valuable conditions for evaluating plant water status using microtensiometers and assessing their performance in a mandarin orchard. Frequent water applications through SDI maintained relatively stable SWC over time, as evidenced by soil moisture sensor data (Fig. 3), while the farmer's 14-day irrigation schedule caused pronounced fluctuations in Ψ_{mt} and, consequently, in soil water content. These contrasting irrigation regimes offered an effective framework to evaluate the sensor's sensitivity in detecting variations in stem water potential under dynamic soil moisture and atmospheric conditions, representative of Mediterranean climates.

Vapour pressure deficit is an environmental variable which, under steady-state SWC conditions, regulates plant water relations and, in turn, stem water potential by affecting leaf transpiration and water transport (Mayr, 2021). In the monitored period, VPD_{max} frequently exceeded 3 kPa and peaked up to 9 kPa, especially in the 2023 season (Fig. 2**c**). On such extreme days, even when the soil water content was not a limiting factor, a prolonged but moderate increase in VPD and air temperature led to hydraulic dysfunctions, including limited stomatal closure, elevated transpiration, and more negative plant water potentials (Schönbeck et al., 2022). These phenomena were observed in the mandarin tree within the SDI plot (Fig. 4**b**, black arrows), in which well-water conditions were ensured by high irrigation frequency, maintaining SWC nearly at the field capacity (Fig. 3**a** and **b**). Exposure to high VPD conditions led to a noticeable decline in Ψ_{pd} values on the following morning compared to pre-event values, suggesting that plants were unable to fully recover overnight from the stress imposed by these extreme atmospheric demands. These results align with those obtained in cotton by Christenson et al. (2024), in which the plants were subjected to continued, high evaporative demand conditions. In our study, the most significant recovery (40.68 %) occurred within the first 24 h, yet full restoration of pre-event levels required up to four days. The observed recovery dynamics align with previous studies on mandarin trees' hydraulic responses under fluctuating atmospheric demands (Dzikiti et al., 2010). Notably, the absence of full recovery in the SPR-irrigated tree (Table 2 and Fig. 4**b**, black arrows) further indicates that less frequent irrigation exacerbates these delays, likely due to insufficient soil water availability.

Under constant SWC conditions, a relatively stable VPD (Fig. 2**a**) satisfactorily drives Ψ_{mt}, especially during the 2022 season (Fig. 8**a**, R^2 =

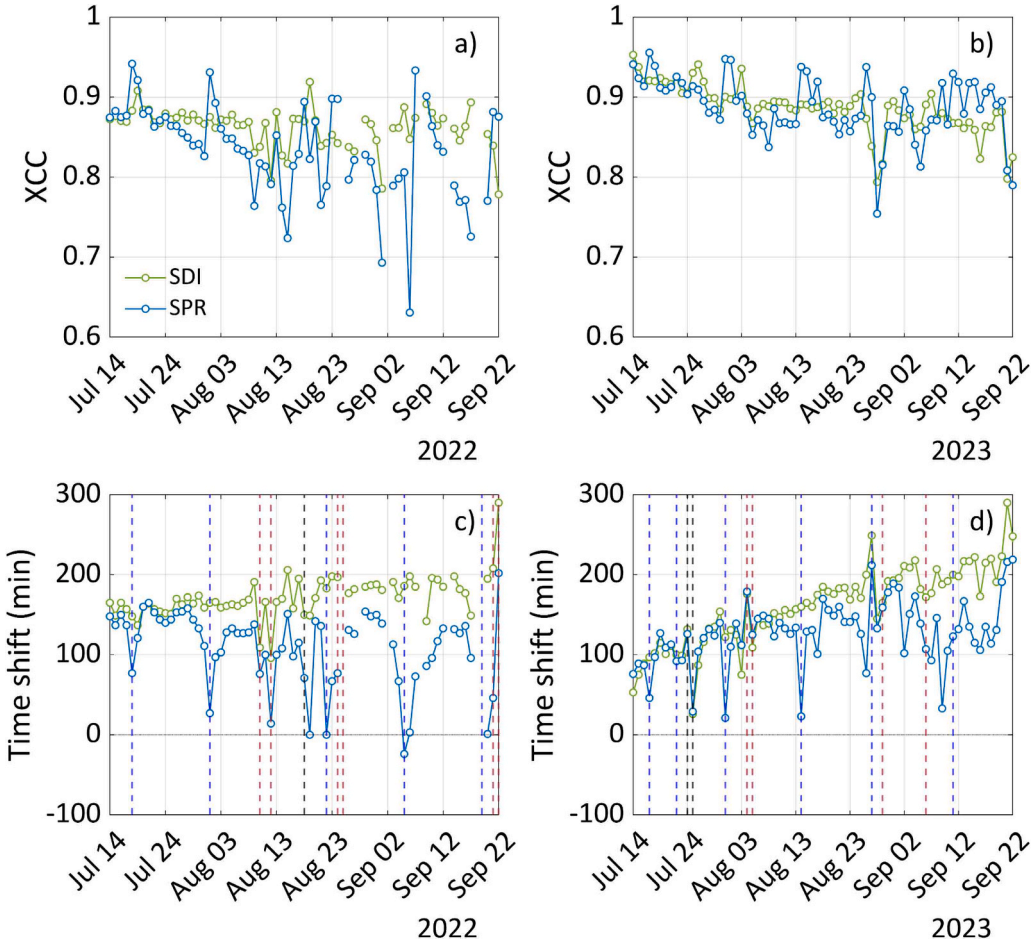

Fig. 9. Daily dynamics of (**a**, **b**) maximum normalised cross-correlation coefficient (XCC) and (**c**, **d**) corresponding time shift between Ψ_{mt} and daily reference evapotranspiration (ETo) under the SDI and SPR irrigation regimes across both seasons. Black dashed lines denote days with $VPD_{max} > 6$ kPa; red dashed lines indicate precipitation events; and blue dashed lines show farmer irrigation events in the SPR plot.

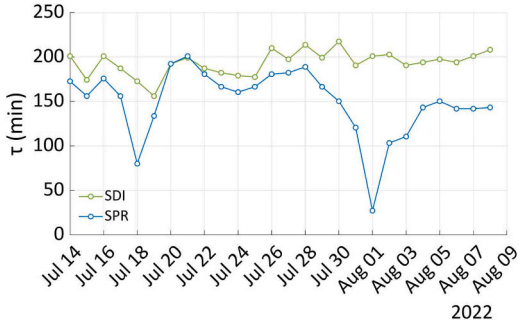

Fig. 10. Daily changes of time constant (τ) for Ψ_{mt} observations under the SDI and SPR irrigation regimes over one SPR irrigation cycle in the 2022 season. Values reported were estimated, in cloudless days, from phase lags obtained by cross-correlation between ETo and Ψ_{mt}.

0.57). These results align with those in well-watered kiwi fruits (Di Biase et al., 2025), pear (Blanco and Kalcsits, 2023), apple (Gonzalez Nieto et al., 2023) and grapevine (Pagay, 2022). Focusing on the refilling phase (Fig. 8**a** and **c**, green ellipse), the correlation between Ψ_{mt} and VPD strengthens considerably, reaching an R^2 of 0.70 in both irrigation seasons. Moreover, it is interesting to note that the separation between morning and afternoon data is preserved, reflecting an underlying hysteresis daily cycle that can be recognised even by pooling all the seasonal data gathered throughout each year of observation, with data dispersed within a well-defined envelope over an approximately elliptical boundary (Fig. 8**a** and **c**). Even if specific data on the hourly-based relationship between Ψ_{mt} and VPD are not available for mandarin, a similar dispersion for the Crop Water Stress Index (CWSI), which is indirectly linked to water potential, can be inferred for this citrus crop (Appiah et al., 2022, Fig. 8). In tree species with significant capacitance effects, such separation can be expected by observing these relations within a short-term diurnal cycle, often showing a hysteresis-like pattern because of the lag between potential transpiration demand and root water uptake (Phillips et al., 1997, 2004; Zhuang et al., 2014).

In contrast, the SPR irrigation regime exhibited weaker correlations between Ψ_{mt} and VPD across the three plant water dynamic phases (Fig. 8**b** and **d**), with a larger scatter and overlap of observations of both the emptying (red dots) and refilling (green dots), suggesting no steady-state condition of SWC was achieved. This variability was particularly evident during the equilibrium phase (Fig. 8**b** and **d**, blue ellipse), where Ψ_{mt} values spanned from well-watered to water-stressed soil moisture conditions. Given that Ψ_{pd} reflects equilibrium between the stem and soil water potential under minimal transpiration (Yang et al., 2013; Zhang et al., 2023), these fluctuations suggest that Ψ_{mt} under the SPR irrigation regime was predominantly influenced by soil water potential rather than atmospheric demand (VPD). During the most water-stressed periods, the SPR irrigated mandarin trees displayed marked physiological responses to the farmer's irrigation events, with Ψ_{pd} recovering up to 40 % of the pre-irrigation value (Table 2) within 24 h post watering, highlighting the tree's capacity to respond rapidly when relieved from severe water deficit. Most of the recovery occurred within the first 24–48 h, after

which the tree's water status improvements plateaued or declined, indicating a limited plant's recovery window. Overall, the ability of trees to rapidly restore physiological processes after irrigation highlights the importance of timely water management in mitigating the impacts of drought and supporting tree health and productivity (Cermak et al., 1993; Jamshidi et al., 2021).

To evaluate the microtensiometers' ability to quantify stem water potentials relative to known and traditional approaches, a comparison was performed with those estimated using a pressure chamber. Diurnal observation of Ψ_{mt} and Ψ_{pc} follows similar daily trends, with slight differences between the MT and PC methods in both irrigation regimes. The Ψ_{pc} consistently recorded more negative values than the Ψ_{mt} ones, particularly during early afternoon when transpiration demand peaked (Fig. 5). However, this discrepancy tends to reduce at higher values of stem water potential (Di Biase et al., 2025; Pagay, 2022; Zucchini et al., 2023), indicating better alignment between the two methods. Our findings showed an average 0.66 MPa offset in the afternoon between Ψ_{pc} and Ψ_{mt}. The lowest Ψ_{mt} values were usually recorded between 16:00 and 17:00, while the lowest Ψ_{pc} values were recorded at 14:00, showing a time-lag regardless of the irrigation regime adopted. Similar lags between Ψ_{mt} and Ψ_{pc} can also be observed in Pagay (2022) for grapevine.

The observed time shift in the Ψ_{mt} response compared to Ψ_{pc} denotes a slower dynamic behaviour, indicating a marked time constant of the microtensiometer, which could be linked to its intrinsic characteristic or the result of the whole complex sensor installation (the sensor itself, the mating paste and wood characteristics), as observed by Lakso et al. (2022). The slow sensor response not only determines a lag in the timing of minimum values but can also be the cause of overestimation of Ψ_{mt} relative to Ψ_{pc}, as a consequence of the smoothing effect exerted by the sensor (or the sensor-tree complex) time constant on the expected true signal of the tree water potential (Ψ_{stem}), acting as a "first-order filter" (similar to a resistance-capacitance network, under the assumption that the Ohm's law analogy holds).

On the contrary, the Ψ_{stem} time-course can be more closely approximated by Ψ_{pc}. While it is arguable that neither Ψ_{mt} or Ψ_{pc} can be assumed as the "true" Ψ_{stem}, since manual readings of water potential (leaf or stem) by pressure chamber is well known to be biased by a significant "operator effect" (Turner, 1985; Levin, 2019), these factors primarily affect only the absolute value of Ψ_{pc} rather than the temporal dynamics. In this sense, differently from Ψ_{mt}, a zero-time lag can be assumed between Ψ_{pc} and the actual Ψ_{stem}.

Sensor time constant (τ) was reported by Lakso et al. (2022) as less than 15 min for the sensor itself; however, the Authors recognise that the τ value of the complex "sensor - mating paste - plant tissue" is difficult to determine, and it may vary on a species- or even plant-basis. Additionally, they highlighted that such an effect could sum up to stem capacitance effects and wood characteristics, to be specifically addressed. A non-zero sensor time constant implies a time lag in Ψ_{mt} vs. Ψ_{pc} readings, particularly during the most dynamic parts of the day when rapid changes in Ψ_{stem} following transpiration demand peaks occur. However, Lakso et al. (2022) reported a good correlation with maximal (pre-dawn) and minimal (afternoon) values (i.e., the values occurring in the less dynamic parts of the day), which are the most relevant values for irrigation management.

In the present study, Ψ_{mt} and Ψ_{pc} in mandarin trees were significantly correlated under both irrigation regimes ($R^2 = 0.62$, $p < 0.0001$, for SDI tree and $R^2 = 0.63$, $p < 0.0001$, for SPR). However, the slopes of the linear regression lines (Fig. 7) deviated from the identity line, indicating a dissimilarity between the two methods. Similar deviations have been reported in other woody crops, such as grapevines (Pagay, 2022), olive orchards (Zucchini et al., 2023) and orange orchards (Vanella et al., 2025). In contrast, near-unity slopes have been observed in smaller or well-watered annual crops, such as nectarines (Conesa et al., 2023) and cotton (Christenson et al., 2024). For cotton, in particular, the stronger agreement could be related to its smaller canopy size, compared to the mandarin tree, which allows microtensiometers to better reflect the whole plant water potential (Blanco and Kalcsits, 2021; Pagay, 2022).

The slopes of the linear regression lines (Fig. 7) observed in our study suggest that Ψ_{mt} changed at a more attenuated extent compared to the Ψ_{pc}, resulting in a systematic overestimation of Ψ_{stem} compared to Ψ_{pc} readings. From a practical point of view, this aspect does not necessarily preclude the use of Ψ_{mt} for irrigation management in mandarin orchards. However, appropriate adjustments are required to account for the low (less-than-one) slope values of the regression lines, as observed under both SDI and SPR irrigation regimes. Similar conclusions were expressed by other Authors (e.g., Pagay, 2022; Conesa et al., 2023) who suggested that, in cases where absolute Ψ_{stem} values are required, the need for crop-specific thresholds is necessary for integrating Ψ_{mt} into irrigation scheduling protocols.

The varying degrees of scattering observed in tree-based measurements, such as Ψ_{mt} vs VPD or ETo, may be linked to the differing levels of dynamic coupling between tree-level processes and changes in atmospheric variables influenced by the irrigation regime. The time lags between tree water potential, estimated by microtensiometer, and atmospheric variables like ETo or VPD create hysteresis-like patterns that may add up to other better-known sources of hysteresis (Wan et al., 2023; Zhuang, 2014; Tuzet et al., 2003; Phillips, 1997). This raises the need for a careful assessment of these effects to evaluate the reliability of microtensiometer data as an indicator of water status in mandarin trees. In this sense, it is necessary to consider the importance of the timing of readings. Lags in diurnal changes in Ψ_{mt} compared to VPD (Fig. 5) or other atmospheric demand variables, such as ETo (Fig. 9), need to be properly addressed, considering both the diurnal and seasonal effects. Hourly Ψ_{mt} values can be used to identify the daily time lag, using the cross-correlation coefficient (Fig. 9). Over the season, a decrease in the maximum cross-correlation coefficient could be observed for both irrigation regimes. Such a decrease paralleled the seasonal reduction of ETo (Fig. 2), but other effects could be involved (Kaner et al., 2020; Phillips et al., 2004; Vogel et al., 2017) since time constant effects can be modulated by changes in physiological aspects other than capacitance (Zhuang et al., 2014).

The substantial time shift and signal attenuation observed across both years make the direct use of raw MT signals as a proxy for Ψ_{stem} challenging. The minimum Ψ_{mt} occurred up to two hours after the observed Ψ_{pc} minimum, while signal attenuation led to systematic overestimation of Ψ_{stem} due to the first-order response characteristics of the sensor-tree complex. Indications of the presence of such features in the dynamic response of MT sensors and about the difference in the technical behaviour of sensors when characterized in laboratory (with a 15-minutes time shift) in comparison to their response when installed on the tree were reported by Lakso et al. (2022), stating the need to consider the output signal as the result of the interaction of the xylem with the sensor and the interfacing compound. Other subsequent studies (Di Biase et al., 2025; Zucchini et al., 2023; Pagay, 2022) reported the presence of such effects and their impact on the correlations between Ψ_{mt} and Ψ_{pc} on different species. In the present study on mandarin citrus, such effects had a large impact on the possibility of a direct comparison of Ψ_{mt} vs. Ψ_{pc}.

At a more general level, directly comparing Ψ_{mt} and Ψ_{pc} in the presence of large time constants would be problematic, particularly on an hourly basis. The predictable differences between signals due to the substantial time shifts observed (up to two hours in this study) would make comparisons with currently published irrigation thresholds of limited practical value. Moreover, a comparison with measurements taken in a specific moment of the day, such as the commonly used "midday" or "pre-dawn" Ψ_{stem}, would discard the valuable time information provided by MTs. Under these ideas, an appropriate characterisation of the dynamic behaviour of the sensor-tree interaction as a composite system could provide a useful insight of trees' condition. In this context, the time constant should not be viewed merely as a hindrance to sensor adoption, but rather as an informative indicator of tree physiological status. Both the time shift and time constant demonstrated

sensitivity to different irrigation regimes in the present study, as shown in Fig. 10. Developing suitable models of the sensor-tree complex's dynamic response to environmental variables would significantly improve the quality of information obtainable from MTs by fully utilising the temporal information provided by the sensors.

Overall, these findings underscore that microtensiometers provide valuable high-resolution monitoring of tree water status, yet their integration into irrigation scheduling protocols requires a sophisticated understanding of the temporal coupling between plant water potential and evaporative demand. This consideration becomes even more critical when attempting to predict stem water potential indirectly from its relationship with environmental drivers such as VPD or ETo, particularly in scenarios where the use of microtensiometers is limited by technical constraints or economic inaccessibility, particularly for small-scale growers.

4.1. Limitations and future research

Continuous MT readings captured stem water potential dynamics with high temporal resolution, demonstrating their potential to rapidly detect physiological responses that could be missed by discrete pressure chamber data. These findings support the use of in situ microtensiometers as reliable tools for real-time irrigation scheduling and stress monitoring under fluctuating environmental conditions. However, several practical limitations were also observed.

In both irrigation seasons, unrealistic Ψ_{mt} values were observed in late September, likely due to water infiltration into the sensor insulation that degraded after 2–3 months of operation. Fig. 11**a** illustrates the MT failure that occurred in 2023 following consecutive rainfall events. Additionally, in 2023, a second monitored mandarin tree under the SDI plot experienced sensor malfunction following the two consecutive days of elevated VPD (Fig. 11**b**, black arrows). The Ψ_{mt} readings deviated from expected patterns, suggesting poor xylem contact or internal disconnection. Notably, reinstallation of the sensor was unsuccessful in restoring signal continuity (Fig. 11**b**, red arrow).

Our findings indicate that predawn Ψ_{mt}, as the most stable indicator unaffected by diurnal or plant-driven fluctuations (i.e., the sensor-tree-complex response), can be used for real-time irrigation management of mandarin orchards in Mediterranean climates under well-watered conditions, with a threshold of -0.51 ± 0.09 MPa. To define physiologically meaningful thresholds of Ψ_{pd} and Ψ_{md} for irrigation scheduling and support the implementation of water-saving strategies such as regulated deficit irrigation, further research is warranted. In particular, a comprehensive assessment incorporating stem water potential, soil water content, and transpiration rate, will be essential to characterise the water status across a range of stress levels (from moderate to severe) and to evaluate the hydraulic responses of mandarin trees under different SWC conditions, such as those observed in the SPR plot, where greater variation in Ψ_{pd} and Ψ_{md} occurs (Table 1).

5. Conclusions

This study demonstrates the potential of microtensiometers as a reliable tool for continuously monitoring stem water potential (Ψ_{stem}) in *C. reticulata* under Mediterranean climate conditions and different irrigation regimes. The high temporal resolution of microtensiometers' readings (Ψ_{mt}) allows the detection of diurnal variations in plant water status, reflecting the combined effect of atmospheric demand, soil water content, and irrigation management. Frequent irrigation via subsurface drip irrigation ensured a more stable Ψ_{mt} and a tighter coupling between plant and atmospheric conditions. Whereas the ordinary low-frequency irrigation scheduling via micro-sprinkler resulted in greater variability and stronger dependence on soil water availability. The comparison between Ψ_{mt} and conventional pressure chamber readings (Ψ_{pc}) revealed a significant correlation, although differences in magnitude and timing were observed. Following an external disturbance induced by shading of the tree, Ψ_{pc} and Ψ_{mt} responded similarly in trend but differed substantially in dynamics, with Ψ_{pc} reacting promptly to microclimate changes, while Ψ_{mt} exhibited a delayed and smoothed response. This delay, quantified through the markedly higher time constant of Ψ_{mt} compared to Ψ_{pc}, reflects the slower response of the microtensiometer sensor-tree complex as a whole, leading to overestimation of Ψ_{stem} when compared to pressure chamber estimations. These findings suggest that the first-order dynamics of the sensor-tree-complex response signal hinder the direct use of Ψ_{mt} as a direct replacement of pressure-chamber Ψ_{stem} measurements. Consequently, compensation protocols accounting for a large time constant should be developed to apply Ψ_{mt} readings to currently published crop-specific Ψ_{stem} thresholds for irrigation scheduling protocols, generally obtained by pressure chamber, that could suitably take into account the full dynamics of the signal. In this respect, the sensitivity shown by Ψ_{mt} time constant to different irrigation regimes and the changes occurring within each irrigation cycle seems to be a promising feature of MTs that could allow for making full use of the timing information provided by the sensor, continuous by nature, in contrast to the point measurements as "midday" and "pre-dawn" water potentials.

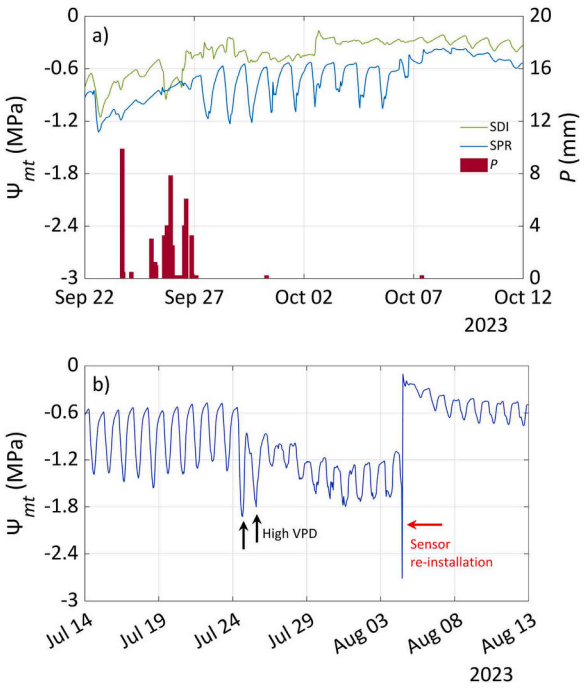

Fig. 11. Observed limitations of MT: **a**) sensor failure following a sequence of precipitation events (*P*) in late September 2023, and **b**) sensor failure following high VPD events (black arrows) for another monitored tree of the SDI plot (red arrow indicates sensor re-installation).

CRediT authorship contribution statement

Antonio Motisi: Writing – review & editing, Visualization, Supervision, Conceptualization. **Girolamo Vaccaro:** Writing – review & editing, Writing – original draft, Visualization, Validation, Methodology, Investigation, Formal analysis, Data curation, Conceptualization. **Mariachiara Fusco:** Writing – review & editing, Visualization, Investigation, Formal analysis, Data curation. **Vincenzo Alagna:** Writing – review & editing, Visualization, Validation, Investigation, Data curation, Conceptualization. **Loris Franco:** Writing – review & editing, Investigation. **Massimo Iovino:** Writing – review & editing, Visualization, Supervision, Conceptualization.

Declaration of Competing Interest

The authors declare that they have no known competing financial interests or personal relationships that could have appeared to influence the work reported in this paper

Acknowledgements

This work is dedicated to the memory of Professor Giuseppe Provenzano, whose vision and commitment led to the establishment of the experimental field where this research was conducted. This work, which stems from one of his original ideas, represents a continuation of his scientific legacy and the values he instilled in that field. We are deeply grateful for his lasting inspiration and contribution. This work was supported by the European Union -FESR or FSE, PON Research and Innovation 2014–2020 -DM 1062/2021 (CUP: B7521002300001), by CN_00000022 "National Research Centre for Agricultural Tecnologies (Agritech)" financed by the D.R. n. 1032 on 17.06.2022, PNRR MUR -M4C2 −1.4 - "Centri Nazionali" - D.D. n. 3138 on 16/12/2021, CUP: B13D21011580004. Spoke 3 Enabling Technologies and sustainable strategies for the smart management of agricultural systems and their environmental impact, and PRIN 2022, "Smart Technologies and Remote Sensing methods to support the sustainable Agriculture WAter Management of Mediterranean woody Crops (SWAM4Crops)", CUP: B53D23018040001.

Data availability

Data will be made available on request.

References

Allen, R.G., Pereira, L.S., Raes, D., Smith, M., 1998. Crop evapotranspiration. FAO Irrig. Drain. Pap. 56, 65–88.

Appiah, S.A., Li, J., Lan, Y., Darko, R.O., Alordzinu, K.E., Al Aasmi, A., Asenso, E., Issaka, F., Afful, E.A., Wang, H., Qiao, S., 2022. Real-Time assessment of mandarin crop water stress index. Sensors 22, 4018. https://doi.org/10.3390/s22114018.

Bader, M.K.F., Ehrenberger, W., Bitter, R., Stevens, J., Miller, B.P., Chopard, J., Rüger, S., Hardy, G.E.S.J., Poot, P., Dixon, K.W., Zimmermann, U., Veneklaas, E.J., 2014. Spatio-temporal water dynamics in mature *banksia menziesii* trees during drought. Physiol. Plant 152, 301–315. https://doi.org/10.1111/ppl.12170.

Ballester, C., Castel, J., Intrigliolo, D.S., Castel, J.R., 2011. Response of clementina de nules citrus trees to summer deficit irrigation. Yield components and fruit composition. Agric. Water Manag 98, 1027–1032. https://doi.org/10.1016/j.agwat.2011.01.011.

Bengtsson, L., Enell, M., 1986. Chem. Anal. Handb. Holocene Palaeoecol. palaeohydrology 423–451.

Blanco, V., Kalcsits, L., 2023. Long-term validation of continuous measurements of trunk water potential and trunk diameter indicate different diurnal patterns for pear under water limitations. Agric. Water Manag 281, 108257. https://doi.org/10.1016/j.agwat.2023.108257.

Bulut, R., Leong, E., 2008. Indirect measurement of suction. Geotech. Geol. Eng. 26, 21–32.

Cahn, M., Hutmacher, R., 2024. Subsurface drip irrigation. Microirrigation for Crop Production. Elsevier Science, pp. 257–301.

Camp, C.R., 1998. Subsurface drip irrigation: a review. Trans. ASAE 41, 1353–1367. https://doi.org/10.13031/2013.17309.

Capurro, M.C., Ham, J.M., Kluitenberg, G.J., Comas, L., Andales, A.A., 2024. A novel sap flow system to measure maize transpiration using a heat pulse method. Agric. Water Manag 301, 108963. https://doi.org/10.1016/j.agwat.2024.108963.

Cermak, J., Matyssek, R., Kucera, J., 1993. Rapid response of large, drought-stressed beech trees to irrigation. Tree Physiol. 12, 281–290. https://doi.org/10.1093/treephys/12.3.281.

Chatfield, C., Xing, H., 2019. Seventh edition. Edn. CRC press. The analysis of time series: an introduction with R. Chapman & Hall/CRC texts in statistical science series. Taylor & Francis Group, Boca Raton.

Choné, X., 2001. Stem water potential is a sensitive indicator of grapevine water status. Ann. Bot. 87, 477–483. https://doi.org/10.1006/anbo.2000.1361.

Christenson, C.G., Gohardoust, M.R., Calleja, S., Thorp, K.R., Tuller, M., Pauli, D., 2024. Monitoring cotton water status with microtensiometers. Irrig. Sci. 42, 995–1011. https://doi.org/10.1007/s00271-024-00930-w.

Ciais, Ph, Reichstein, M., Viovy, N., Granier, A., Ogée, J., Allard, V., Aubinet, M., Buchmann, N., Bernhofer, Chr, Carrara, A., Chevallier, F., De Noblet, N., Friend, A.D., Friedlingstein, P., Grünwald, T., Heinesch, B., Keronen, P., Knohl, A., Krinner, G., Loustau, D., Manca, G., Matteucci, G., Miglietta, F., Ourcival, J.M., Papale, D., Pilegaard, K., Rambal, S., Seufert, G., Soussana, J.F., Sanz, M.J., Schulze, E.D., Vesala, T., Valentini, R., 2005. Europe-wide reduction in primary productivity caused by the heat and drought in 2003. Nature 437, 529–533. https://doi.org/10.1038/nature03972.

Clearwater, M.J., Goldstein, G., 2005. Embolism repair and long distance water transport. in: Vascular Transport in Plants. Elsevier, pp. 375–399. https://doi.org/10.1016/B978-012088457-5/50020-4.

Conesa, M.R., Conejero, W., Vera, J., Ruiz-Sánchez, M.C., 2023. Assessment of trunk microtensiometer as a novel biosensor to continuously monitor plant water status in nectarine trees. Front. Plant Sci. 14, 1123045. https://doi.org/10.3389/fpls.2023.1123045.

Dainese, R., De Cfl Lopes, B., Tedeschi, G., Lamarque, L.J., Delzon, S., Fourcaud, T., Tarantino, A., 2022. Cross-validation of the high-capacity tensiometer and thermocouple psychrometer for continuous monitoring of xylem water potential in saplings. J. Exp. Bot. 73, 400–412. https://doi.org/10.1093/jxb/erab412.

Dane, J.H., Hopmans, J.W., Topp, G.C., 2002. Pressure plate extractor. Methods of soil analysis: physical methods. Soil Science Society of America, Madison, pp. 688–690.

Dean, W.E., 1974. Determination of carbonate and organic matter in calcareous sediments and sedimentary rocks by loss on ignition; comparison with other methods. J. Sediment. Res. 44 (1), 242–248.

Di Biase, R., Calabritto, M., Mininni, A.N., Montanaro, G., Dichio, B., 2025. Microtensiometer-based trunk water potential as a plant water status indicator in kiwifruit under different soil water availability. Irrig. Sci. https://doi.org/10.1007/s00271-025-01020-1.

Dzikiti, S., Verreynne, J.S., Stuckens, J., Strever, A., Verstraeten, W.W., Swennen, R., Coppin, P., 2010. Determining the water status of satsuma mandarin trees [Citrus Unshiu Marcovitch] using spectral indices and by combining hyperspectral and physiological data. Agric. For. Meteor. 150, 369–379. https://doi.org/10.1016/j.agrformet.2009.12.005.

Fernández, J.E., 2014. Plant-based sensing to monitor water stress: applicability to commercial orchards. Agric. Water Manag.

Galindo, A., Collado-González, J., Griñán, I., Corell, M., Centeno, A., Martín-Palomo, M.J., Girón, I.F., Rodríguez, P., Cruz, Z.N., Memmi, H., Carbonell-Barrachina, A.A., Hernández, F., Torrecillas, A., Moriana, A., Pérez-López, D., 2018. Deficit irrigation and emerging fruit crops as a strategy to save water in Mediterranean semiarid agrosystems. Agric. Water Manag 202, 311–324. https://doi.org/10.1016/j.agwat.2017.08.015.

García-Tejero, I., Romero-Vicente, R., Jiménez-Bocanegra, J.A., Martínez-García, G., Durán-Zuazo, V.H., Muriel-Fernández, J.L., 2010. Response of citrus trees to deficit irrigation during different phenological periods in relation to yield, fruit quality, and water productivity. Agric. Water Manag 97, 689–699. https://doi.org/10.1016/j.agwat.2009.12.012.

Gonzalez Nieto, L., Huber, A., Gao, R., Biasuz, E.C., Cheng, L., Stroock, A.D., Lakso, A.N., Robinson, T.L., 2023. Trunk water potential measured with microtensiometers for managing water stress in "Gala" apple trees. Plants 12, 1912. https://doi.org/10.3390/plants12091912.

Gonzalez-Altozano, P., Castel, J.R., 1999. Regulated deficit irrigation in 'Clementina de Nules' citrus trees. I. yield and fruit quality effects. J. Hortic. Sci. Biotechnol. 74 (6), 706–713.

Hacke, U.G., Sperry, J.S., 2001. Functional and ecological xylem anatomy. Perspect. Plant Ecol. Evol. Syst. 4 (2), 97–115.

Jamshidi, S., Zand-Parsa, S., Niyogi, D., 2021. Physiological responses of Orange trees subject to regulated deficit irrigation and partial root drying. Irrig. Sci. 39, 441–455. https://doi.org/10.1007/s00271-020-00709-9.

Jones, H.G., 2004. Irrigation scheduling: advantages and pitfalls of plant-based methods. J. Exp. Bot. 55, 2427–2436. https://doi.org/10.1093/jxb/erh213.

Kaner, A., Preisler, Y., Grünzweig, J.M., Mau, Y., 2020. Internal water storage buffering maintains plant function under drought as described by a general hydraulic model. https://doi.org/10.1101/2020.02.11.943563.

Lakso, A.N., Santiago, M., Stroock, A.D., 2022. Monitoring stem water potential with an embedded microtensiometer to inform irrigation scheduling in fruit crops. Horticulturae 8, 1207. https://doi.org/10.3390/horticulturae8121207.

Lamm, F.R., Colaizzi, P.D., Sorensen, R.B., Bordovsky, J.P., Dougherty, M., Balkcom, K., Zaccaria, D., Bali, K.M., Rudnick, D.R., Peters, R.T., 2021. A 2020 vision of subsurface drip irrigation in the U.S. Trans. ASABE 64, 1319–1343. https://doi.org/10.13031/trans.14555.

Levin, A.D., 2019. Re-evaluating pressure chamber methods of water status determination in field-grown grapevine (Vitis spp.). Agric. Water Manag 221, 422–429. https://doi.org/10.1016/j.agwat.2019.03.026.

Lundblad, M., Lagergren, F., Lindroth, A., 2001. Evaluation of heat balance and heat dissipation methods for sapflow measurements in pine and spruce. Ann. For. Sci. 58, 625–638. https://doi.org/10.1051/forest:2001150.

Mancha, L., Uriarte, D., Prieto, M., 2021. Characterization of the transpiration of a vineyard under different irrigation strategies using sap flow sensors. Water 13, 2867. https://doi.org/10.3390/w13202867.

Martínez-Gimeno, M.A., Castiella, M., Rüger, S., Intrigliolo, D.S., Ballester, C., 2017. Evaluating the usefulness of continuous leaf turgor pressure measurements for the assessment of persimmon tree water status. Irrig. Sci. 35, 159–167. https://doi.org/10.1007/s00271-016-0527-3.

Mayr, S., 2021. Relevance of time and spatial scales in plant hydraulics. Tree Physiol. 41, 1781–1784. https://doi.org/10.1093/treephys/tpab093.

Monteith, J.L., Unsworth, M.H., 2008. Principles of environmental physics. Plants, animals, and the atmosphere. Academic Press.

Nobel, P.S., 2009. Physicochemical and Environmental Plant Physiology. Fourth edition. Chapter 9 - Plants and Fluxes, Pages 438-505. Academic Press.

Ortuño, M.F., García-Orellana, Y., Conejero, W., Ruiz-Sánchez, M.C., Alarcón, J.J., Torrecillas, A., 2006. Stem and leaf water potentials, gas exchange, sap flow, and

trunk diameter fluctuations for detecting water stress in lemon trees. Trees 20, 1–8. https://doi.org/10.1007/s00468-005-0004-8.
Pagay, V., 2022. Evaluating a novel microtensiometer for continuous trunk water potential measurements in field-grown irrigated grapevines. Irrig. Sci. 40, 45–54. https://doi.org/10.1007/s00271-021-00758-8.
Pagay, V., Santiago, M., Sessoms, D.A., Huber, E.J., Vincent, O., Pharkya, A., Corso, T.N., Lakso, A.N., Stroock, A.D., 2014. A microtensiometer capable of measuring water potentials below -10 MPa. Lab Chip 14, 2806–2817. https://doi.org/10.1039/C4LC00342J.
Phillips, N., Nagchaudhuri, A., Oren, R., Katul, G., 1997. Time constant for water transport in loblolly pine trees estimated from time series of evaporative demand and stem sapflow. Trees 11, 412. https://doi.org/10.1007/s004680050102.
Phillips, N.G., Oren, R., Licata, J., Linder, S., 2004. Time series diagnosis of tree hydraulic characteristics. Tree Physiol. 24, 879–890. https://doi.org/10.1093/treephys/24.8.879.
Poggi, I., Polidori, J.J., Gandoin, J.M., Paolacci, V., Battini, M., Albertini, M., Améglio, T., Cochard, H., 2007. Stomatal regulation and xylem cavitation in clementine (*citrus clementina* Hort) under drought conditions. J. Hortic. Sci. Biotechnol. 82 (6), 845–848. https://doi.org/10.1080/14620316.2007.11512316.
Provenzano, G., 2007. Using HYDRUS-2D simulation model to evaluate wetted soil volume in subsurface drip irrigation systems. J. Irrig. Drain. Eng. 133, 342–349. https://doi.org/10.1061/(ASCE)0733-9437(2007)133:4(342).
Quick, D.D., Espino, S., Morua, M.G., Schenk, H.J. 2016. Effects of thermal gradients in sapwood on stem psychrometry. In International Symposium on Sensing Plant Water Status-Methods and Applications in Horticultural Science 1197 (pp. 23-30).
Rabbel, I., Diekkrüger, B., Voigt, H., Neuwirth, B., 2016. Comparing ΔTmax determination approaches for Granier-Based sapflow estimations. Sensors 16, 2042. https://doi.org/10.3390/s16122042.
Rallo, G., González-Altozano, P., Manzano-Juárez, J., Provenzano, G., 2017. Using field measurements and FAO-56 model to assess the eco-physiological response of citrus orchards under regulated deficit irrigation. Agric. Water Manag 180, 136–147. https://doi.org/10.1016/j.agwat.2016.11.011.
Ravikumar, V., 2023. Cham. Sprinkler and drip irrigation: theory and practice. Springer Nature.
Rawlins, S.L., 1966. Theory for thermocouple psychrometers used to measure water potential in soil and plant samples. Agric. Meteorol. 3 (5-6), 293–310.
Romero-Trigueros, C., Gambín, J.M.B., Nortes Tortosa, P.A., Cabañero, J.J.A., Nicolás Nicolás, E., 2021. Isohydricity of two different citrus species under deficit irrigation and reclaimed water conditions. Plants 10, 2121. https://doi.org/10.3390/plants10102121.
Scholander, P.F., Bradstreet, E.D., Hemmingsen, E.A., Hammel, H.T., 1965. Sap pressure in vascular plants: negative hydrostatic pressure can be measured in plants. Science 148, 339–346. https://doi.org/10.1126/science.148.3668.339.
Schönbeck, L.C., Schuler, P., Lehmann, M.M., Mas, E., Mekarni, L., Pivovaroff, A.L., Turberg, P., Grossiord, C., 2022. Increasing temperature and vapour pressure deficit lead to hydraulic damages in the absence of soil drought. Plant Cell Environ. 45, 3275–3289. https://doi.org/10.1111/pce.14425.
Singh, V.P., Su, Q., 2022. Irrigation engineering. Principles, processes, procedures, design, and management. Cambridge University Press, Cambridge.
Turner, N.C., 1988. Measurement of plant water status by the pressure chamber technique. Irrig. Sci. 9, 289–308. https://doi.org/10.1007/BF00296704.
Tuzet, A., Perrier, A., Leuning, R., 2003. A coupled model of stomatal conductance, photosynthesis and transpiration. Plant Cell Environ. 26, 1097–1116. https://doi.org/10.1046/j.1365-3040.2003.01035.x.
Vanella, D., Guarrera, S., Ferlito, F., Longo-Minnolo, G., Milani, M., Pappalardo, G., Nicolosi, E., Giuffrida, A.G., Torrisi, B., Las Casas, G., Consoli, S., 2025. Effects of organic mulching and regulated deficit irrigation on crop water status, soil and yield features in an Orange orchard under Mediterranean climate. Sci. Total Environ. 958, 177528. https://doi.org/10.1016/j.scitotenv.2024.177528.
Venturin, A.Z., Guimarães, C.M., Sousa, E.F.D., Machado Filho, J.A., Rodrigues, W.P., Serrazine, Í.D.A., Bressan-Smith, R., Marciano, C.R., Campostrini, E., 2020. Using a crop water stress index based on a sap flow method to estimate water status in conilon coffee plants. Agric. Water Manag 241, 106343. https://doi.org/10.1016/j.agwat.2020.106343.
Vogel, T., Votrubova, J., Dohnal, M., Dusek, J., 2017. A simple representation of plant water storage effects in coupled soil water flow and transpiration stream modeling. Vadose Zone J. 16, 1–10. https://doi.org/10.2136/vzj2016.12.0128.
Wan, L., Zhang, Q., Cheng, L., Liu, Y., Qin, S., Xu, J., Wang, Y., 2023. What determines the time lags of sap flux with solar radiation and vapor pressure deficit? Agric. For. Meteor. 333, 109414. https://doi.org/10.1016/j.agrformet.2023.109414.
Yang, Y., Guan, H., Hutson, J.L., Wang, H., Ewenz, C., Shang, S., Simmons, C.T., 2013. Examination and parameterization of the root water uptake model from stem water potential and sap flow measurements. Hydrol. Process 27, 2857–2863. https://doi.org/10.1002/hyp.9406.
Ye, M., Zhao, X., Biswas, A., Huo, G., Yang, B., Zou, Y., Siddique, K.H.M., Gao, X., 2021. Measurements and modeling of hydrological responses to summer pruning in dryland apple orchards. J. Hydrol. 594, 125651. https://doi.org/10.1016/j.jhydrol.2020.125651.
Zhang, X., Yang, H., Shukla, M.K., Du, T., 2023. Proposing a crop-water-salt production function based on plant response to stem water potential. Agric. Water Manag 278, 108162. https://doi.org/10.1016/j.agwat.2023.108162.
Zhuang, J., Yu, G.-R., Nakayama, K., 2014. A series RCL circuit theory for analyzing Non-Steady-State water uptake of maize plants. Sci. Rep. 4, 6720. https://doi.org/10.1038/srep06720.
Zimmermann, D., Reuss, R., Westhoff, M., Geßner, P., Bauer, W., Bamberg, E., Bentrup, F.-W., Zimmermann, U., 2008. A novel, non-invasive, online-monitoring, versatile and easy plant-based probe for measuring leaf water status. J. Exp. Bot. 59, 3157–3167. https://doi.org/10.1093/jxb/ern171.
Zucchini, M., Guzmán-Delgado, P., Santos, E., Synstelien, T., Marino, G., 2023. Preliminary observations on the use of microtensiometers to continuously measure water potential in a mature olive orchard, in: 2023 IEEE International Workshop on Metrology for Agriculture and Forestry (MetroAgriFor). Presented at the 2023 IEEE International Workshop on Metrology for Agriculture and Forestry (MetroAgriFor), IEEE, Pisa, Italy, pp. 268–272. https://doi.org/10.1109/MetroAgriFor58484.2023.10424405.